frontiers | Frontiers in Materials

TYPE Original Research
PUBLISHED 03 December 2025
DOI 10.3389/fmats.2025.1714941

OPEN ACCESS

EDITED BY
Jie Xu,
Tianjin University, China

REVIEWED BY
Mohammad M. Karimi,
Tarbiat Modares University, Iran
Daming Wang,
Nanjing Forestry University, China

*CORRESPONDENCE
Chaozhe Jiang,
lyktougao00@163.com

RECEIVED 28 September 2025
REVISED 10 November 2025
ACCEPTED 13 November 2025
PUBLISHED 03 December 2025

CITATION
Yang M, Li S, Guo X, Pu M, Li C, Xu O, Wu S, Jiang C, Li Y, Mao H, Zhong L and A W (2025) Microstructural engineering of high-content rubber asphalt via precision devulcanization for enhanced performance.
Front. Mater. 12:1714941.
doi: 10.3389/fmats.2025.1714941

Microstructural engineering of high-content rubber asphalt via precision devulcanization for enhanced performance

Meng Yang[1], Shanyuan Li[1], Xiaohong Guo[1], Mingyan Pu[1], Chongyuan Li[1], Ouyang Xu[1], Shibing Wu[1], Chaozhe Jiang[2,3]*, Yukun Li[4], Hanqing Mao[5], Lei Zhong[4] and Wenqian A[3]

[1]General Section of Haixi Highway Qinghai Province, Haixi, Qinghai, China, [2]Department of Civil and Environmental Engineering, University of Waterloo, Waterloo, ON, Canada, [3]School of Transportation and Logistics, Southwest Jiaotong University, Chengdu, China, [4]School of Civil Engineering, Southwest Jiaotong University, Chengdu, China, [5]Qinghai Provincial Department of Transportation, Xining, China

Introduction: The practical deployment of high-content rubberized asphalt is often hindered by its compromised workability and unstable performance. Moving beyond conventional devulcanization approaches, this study introduces an integrated strategy of interface-controlled devulcanization and microstructural tailoring to address these challenges.

Methods: A bespoke devulcanizing agent (RubberSynth-AP) was synthesized to promote selective scission of sulfur-based crosslinks and improve interfacial adhesion. Coupled with an optimized production process, this method allows the stable integration of crumb rubber at concentrations up to 30% by binder weight. Multi-scale rheological analyses—encompassing temperature sweeps, multiple stress creep recovery (MSCR), and linear amplitude sweep (LAS) tests—were employed.

Results: An optimum rubber content of 26% was identified, exhibiting a superior combination of properties: a failure temperature of 76.5 °C, 40% lower viscosity, 53.12% recovery rate, and enhanced fatigue resistance. Mechanistic analysis uncovered a microstructural evolution from a heterogeneous, stress-concentrating system to a homogeneous, elastic-network-dominated morphology. This structural improvement supported the adoption of a dense-graded AC-13 mixture design, achieving a remarkable dynamic stability of 3,850 cycles/mm. Economically and environmentally, this technique promotes the consumption of 18 tons of waste rubber per lane-kilometer with a cost reduction of approximately ¥17,000.

Discussion: Collectively, this study demonstrates that the interface-controlled devulcanization strategy enables the production of high-content rubberized asphalt (up to 30%) with superior and balanced rheological properties, overcoming the longstanding workability-performance trade-off. The findings provide a scientifically-grounded and economically viable solution for developing sustainable pavement materials.

KEYWORDS

devulcanized rubber asphalt, controlled devulcanization, interfacial compatibility, multi-scale characterization, sustainable pavement materials

1 Introduction

The continuous expansion of global transportation infrastructure, coupled with the advancing principles of sustainable development, has placed unprecedented demands on the resource circularity and environmental compatibility of road construction materials (Putra Jaya et al., 2021). In this context, waste tire rubber powder-modified asphalt technology is regarded as one of the most promising green pavement solutions due to its significant advantages in enhancing pavement performance—including fatigue resistance, aging resistance (Yao et al., 2023), and driving comfort—while enabling the large-scale, high-value utilization of waste tire resources. Consequently, it has attracted widespread attention from both academic and engineering communities worldwide (Li et al., 2025; Zhang et al., 2024a).

The incorporation of crumb rubber modifier (CRM) into the asphalt system not only enhances road performance but also helps alleviate the increasingly severe issue of "black pollution," thereby aligning with the core principles of the circular economy and carbon emission reduction strategies (Zhang et al., 2024b; Yang et al., 2022; Zhang et al., 2024c; Zhao et al., 2023). Wang et al. (2017) systematically reviewed recent advancements in rubberized asphalt, including preparation techniques, rheological properties, storage stability, and modification mechanisms. Their study summarized strategies for improving the compatibility between crumb rubber and asphalt through chemical methods (e.g., activation and devulcanization), which effectively enhance the high- and low-temperature performance and durability of crumb rubber-modified asphalt (CRMA). Gamboa et al. (2021) employed a life cycle assessment (LCA) methodology to compare rubberized asphalt pavement with conventional asphalt (CA) pavement. Their results demonstrated that rubberized asphalt (RA) is a more environmentally friendly alternative to CA, as it requires fewer virgin raw materials and can reduce the overall production of mixture over the pavement's life cycle due to its superior performance, which necessitates less maintenance and fewer repairs.

From a materials science perspective, the incorporation of rubber particles significantly enhances the viscoelastic properties and damage tolerance of asphalt through the formation of a unique, three-dimensional elastic network structure (Su et al., 2024; Payungwong et al., 2024; Picado-Santos et al., 2020). From an environmental perspective, the utilization of one ton of crumb rubber is equivalent to recycling approximately 30 car tires, thereby yielding substantial social and ecological benefits (Gkyrtis and Pomoni, 2024). However, despite decades of development, the large-scale engineering application of high-content crumb rubber-modified asphalt (typically defined by a crumb rubber content exceeding 20% by weight) still faces significant challenges. These limitations necessitate in-depth research and systematic resolution (Liu et al., 2023; Xu et al., 2023; Wang et al., 2024a).

The primary technical bottleneck restricting the large-scale application of high-content rubberized asphalt is rooted in its inherent material properties, which manifest in three key aspects (Wang et al., 2020): first, processing performance. The incorporation of a high content of rubber particles induces an exponential increase in the high-temperature viscosity of the asphalt binder, necessitating an increase in mixing temperature of 20 °C–30 °C. This elevation not only raises energy consumption and emissions of harmful gases but also accelerates the aging of the asphalt itself (Wang et al., 2024b). Wang et al. (2022) analyzed the effects of high-content crumb rubber and different preparation methods on the properties of asphalt under various aging conditions. Their results indicated that as aging progresses, the crumb rubber (CR) in high-content rubber-modified asphalt (HCRMA) continuously undergoes devulcanization and degradation reactions, leading to the release of silica and S–C bonded substances from the CR into the asphalt phase. The elasticity of HCRMA was found to initially decrease and then increase with the degree of aging. Second, material stability. The density difference and chemical property disparity between the crumb rubber and the asphalt matrix render the binder highly prone to phase separation during thermal storage, resulting in reduced modification effectiveness and uneven performance (Sienkiewicz et al., 2017). Qiao et al. (2025) investigated the rheological properties and storage stability of high-content rubber-modified asphalt. Their results showed that sulfur-containing compounds can simultaneously enhance both the high- and low-temperature rheological properties but reduce the solubility of the crumb rubber, leading to an increase in viscosity. During thermal storage, the dominant separation mechanism is the settlement of crumb rubber particles. Higher storage temperatures exacerbate this settlement, intensifying phase separation and reducing the storage stability of HCRMA. Third, mixture performance (Wu et al., 2023). The gap-graded aggregate design, commonly adopted to improve workability, often leads to difficulties in compaction, excessively high air void content, and instability in the mineral skeleton structure, which ultimately

TABLE 1 Test results of basic technical properties of SK90 asphalt.

Indicator		Unit	Test result	Specification requirement
Penetration at 25 °C, 100 g, 5 s		0.1 mm	85.0	80~100
Ductility at 15 °C		cm	138.0	≥100
Softening point		°C	48.6	≥44
Residue after RTFOT	Mass loss	0.5	0.6	≤0.8
	Retained penetration ratio at 25 °C	73.1	73.5	≥57
	Retained ductility at 15 °C	20.9	22.6	≥8

TABLE 2 Basic performance test results of rubber powder.

Test indicator	Unit	Measured value	Specification limit
Rubber content	%	58.00	≥42
Carbon black content	%	31.03	≥28
Acetone extract content	%	7.56	≤22
Ash content	%	4.77	≤8
Fiber content	%	0.01	<1
Metal content	%	0.02	<0.03
Moisture content	%	0.1	<1
Relative density	-	1.270	1.10~1.30

TABLE 3 Test results of basic properties of aggregates.

Test indicator	Unit	Measured value	Specification limit
Apparent relative density	-	2.956	≥2.60
Aggregate crushing value	%	14.1	≤26
Water absorption	%	0.46	≤2.0
Los Angeles Abrasion loss	%	18.8	≤28

TABLE 4 Basic properties test results of mineral powder.

Test indicator	Unit	Measured value	Specification limit
Apparent density	g/cm^3	2.663	≥2.50
Moisture content	%	0.2	≤1
Particle size range	<0.6 mm	100	100
Particle size range	<0.15 mm	98.5	90~100
Particle size range	<0.075 mm	93.6	75~100
Appearance	-	No agglomerates	No agglomerates
Hydrophilic coefficient	-	0.40	<1
Plasticity index	%	2.5	<4

undermines the long-term service performance of the pavement (Arabani et al., 2018). These interwoven factors collectively restrict the large-scale application of high-content rubberized asphalt in practical engineering. Duan et al. (2022) systematically reviewed research trends in rubberized asphalt and its mixtures with different crumb rubber content levels. Their review compared and evaluated the preparation techniques, modification mechanisms, and comprehensive performance of various rubberized asphalt binders and mixtures, indicating that excessively high crumb rubber content can also hinder mixture compaction and reduce moisture stability.

To overcome these technical bottlenecks, researchers have attempted to use devulcanizing agents to induce the degradation of crumb rubber, disrupting its three-dimensional cross-linked network structure to improve its dispersibility and compatibility in asphalt. Existing devulcanization systems primarily include disulfides, polysulfides, amine compounds, and organic acids (Zhang et al., 2022). However, although these traditional

TABLE 5 Gradation composition of crumb rubber modified asphalt mixture AC-13.

AC-13	Passing percentage by mass through following sieves (mm) (%)									
Sieve size	16	13.2	9.5	4.75	2.36	1.18	0.6	0.3	0.15	0.075
Upper limit of gradation	100	100	85	68	50	38	28	20	15	8
Lower limit of gradation	100	90	68	38	24	15	10	7	5	4
Median gradation	100	95	76.5	53	37	26.5	19	13.5	10	6
Selected gradation	100	95	79	47	30	20	16	11	9	6

TABLE 6 Optimal asphalt binder contents for different asphalt binders.

Asphalt type	Optimal asphalt-aggregate ratio (%)
22SRA-3h	5.8
26SRA-3h	6.0
30SRA-3h	6.5
MA	5.1
22RA-3h	6.6

devulcanizing agents can promote degradation to some extent, they suffer from significant drawbacks: (1) low devulcanization efficiency and an inability to achieve selective cleavage of cross-links (Zhang et al., 2023a); (2) poor compatibility with asphalt components, often leading to phase separation (Zhou et al., 2024); (3) a severe loss of high-temperature performance, where improvements in workability are often achieved at the expense of rutting resistance (Zhou et al., 2024a); (4) narrow processing windows, requiring strict control over temperature and time (Kabir et al., 2021); and (5) a limited ability to increase the crumb rubber content, making it difficult to surpass the 25% threshold (Obukhova et al., 2024). More fundamentally, existing research lacks a systematic understanding of several critical aspects: the evolution mechanism of the crumb rubber network structure during devulcanization (Zhang et al., 2019); the chemical composition and interfacial behavior of the degradation products (Han et al., 2016); the response patterns of multi-scale rheological properties; and the characteristics of long-term performance evolution (Xu et al., 2021). In particular, there is a lack of in-depth understanding of the structure-property relationship between microstructural evolution and macroscopic performance (Gao et al., 2025). This renders the modification process akin to a "black box," where performance improvements rely more on empirical trial and error than on precise design (Zhao et al., 2024).

At the mixture design level, a complete design theory and methodology system suitable for devulcanized rubberized asphalt has yet to be established. Current performance evaluation still relies excessively on traditional empirical indicators, such as penetration and softening point, which are inadequate for accurately characterizing the nonlinear mechanical response and damage evolution of materials under high-stress, varying-temperature, and long-term aging conditions (Zhang et al., 2023b). Furthermore, research on the design of volumetric parameters, gradation optimization, and performance prediction for mixtures incorporating devulcanized rubber remains insufficient. Moreover, there is a lack of systematic design guidelines and standard specifications (Zhou et al., 2024b).

Based on the aforementioned research status and technical bottlenecks, this study moves beyond the traditional "devulcanization-only" approach and proposes an integrated technical pathway of "controlled devulcanization–interface stabilization–performance synergy." The core innovation lies in the development of a novel devulcanizing agent through rational molecular design, which aims to achieve precise cleavage of sulfur cross-links (S–S and C–S) while effectively inhibiting the re-cross-linking of cleaved free radicals. This approach facilitates the breakdown of the three-dimensional network structure while simultaneously promoting the formation of a stable and compatible transition layer at the rubber-asphalt interface. This study will systematically elucidate the influence patterns and underlying mechanisms of key parameters—including crumb rubber content and devulcanization time—on the material's microstructural evolution, viscoelastic properties, damage behavior, and long-term durability. A multi-scale performance evaluation and prediction system will be established, integrating advanced rheological characterization methods such as dynamic shear rheometry (DSR), multiple stress creep recovery (MSCR), and linear amplitude sweep (LAS). Innovatively, a new mixture design method for devulcanized rubberized asphalt, based on AC-type dense gradation, is proposed to resolve the inherent contradiction between workability and pavement performance, thereby achieving their synergistic optimization.

This research aims to provide a solid theoretical foundation and reliable technical support for the material design, process optimization, performance evaluation, and engineering application of high-content devulcanized rubber-modified asphalt (HDRMA). The outcomes are expected to drive the innovative development and practical application of green, low-carbon pavement materials, thereby offering new technical pathways and solutions for the sustainable development of transportation infrastructure.

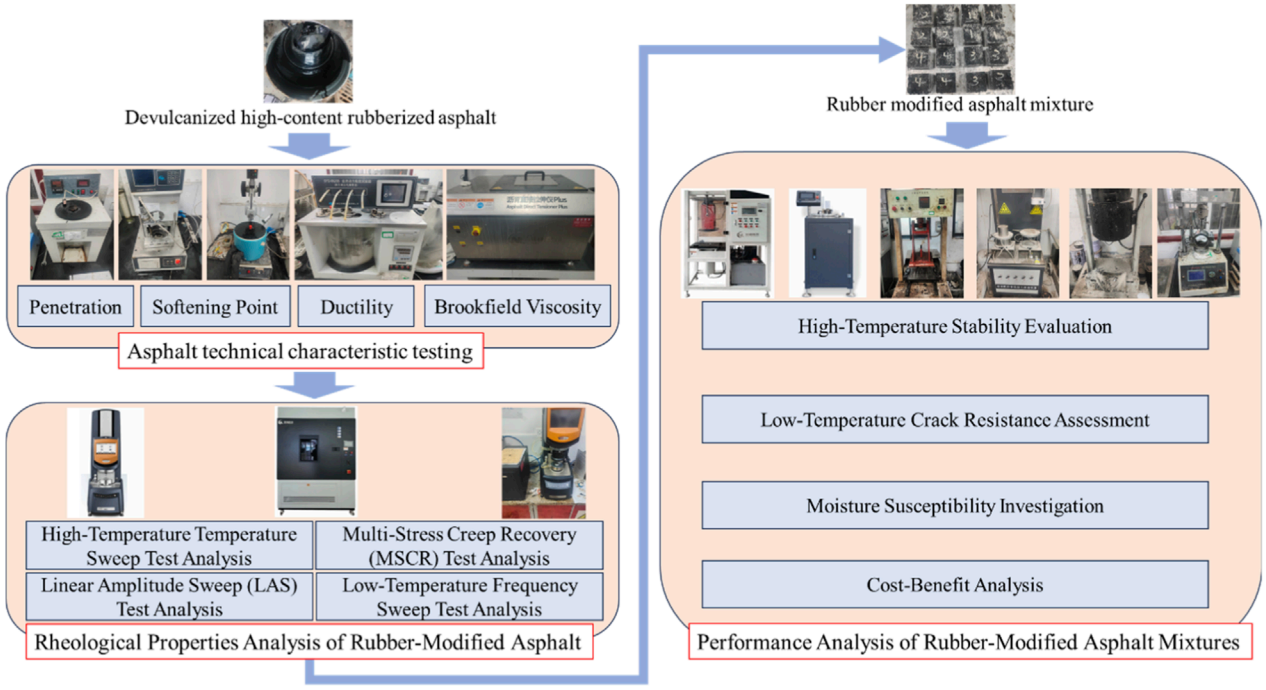

FIGURE 1
Multi-scale characterization technical system for high-content rubber asphalt and its mixtures.

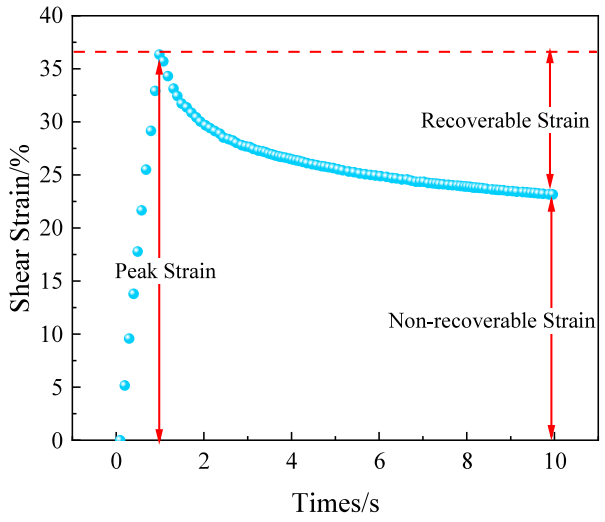

FIGURE 2
Typical creep and recovery behavior of high-content cracked rubber asphalt.

2 Materials and methods

2.1 Materials

2.1.1 Base asphalt

The chemical composition of the base asphalt, particularly its content of light fractions, is a critical determinant for the swelling and subsequent degradation of crumb rubber (CR). To meet the specific requirements of the devulcanization mechanism in high-content rubber asphalt, SK-90 asphalt was selected following a comparative analysis of several base asphalts. A key characteristic of this asphalt is its high aromatics content (32.5%), which provides a favorable environment for the thorough penetration and controlled degradation of rubber particles. An appropriate ratio of saturates to resins ensures system stability during the aggressive devulcanization process. The fundamental technical properties of the SK-90 asphalt are summarized in Table 1, confirming its suitability for the preparation of high-content rubber asphalt.

2.1.2 Crumb rubber modifier (CRM)

According to the Chinese transportation industry standard JT/T 797-2011, vulcanized crumb rubber from waste tires is classified into three categories based on particle size. Engineering practice and fundamental principles of mass transfer suggest that Class II rubber powder exhibits an optimal balance of properties for asphalt modification. This moderate particle size distribution influences both the dispersion of the rubber particles within the asphalt matrix and the ultimate physico-mechanical properties of the composite. To achieve a high degree of devulcanization while maintaining a reinforcing effect, 40-mesh rubber powder was systematically evaluated and selected for this study. Its key properties, as listed in Table 2, meet all relevant specification requirements.

2.1.3 Devulcanizing agent

As a functional additive, the devulcanizing agent is pivotal in enhancing modification efficiency through a dual mechanism:

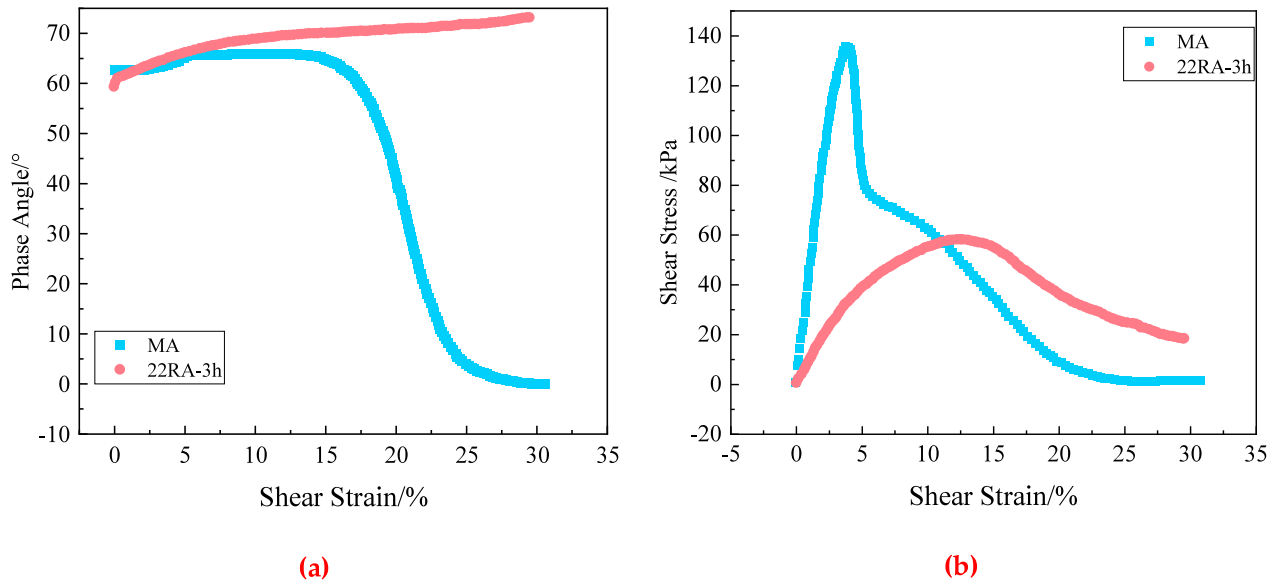

FIGURE 3
(a) Phase angle and **(b)** shear stress versus shear strain.

(1) catalytically cleaving sulfur-based cross-linking bonds (S–S and C–S) within the rubber network, and (2) capturing free radicals to inhibit re-crosslinking. This study selected three agents for comparative testing: a novel agent, RubberSynth-AP, which was independently developed by our research team, and two commercially available reference agents, DA-1 and DA-2. Through unique molecular design, RubberSynth-AP is engineered to exhibit superior catalytic efficiency under the specified processing temperature of 200 °C, promoting not only efficient devulcanization but also the formation of stable olefinic structures that enhance compatibility with the asphalt phase. The detailed chemical composition is proprietary and protected for patent reasons; however, its efficacy is comparatively evaluated against commercial agents in this study to demonstrate its superior performance in selective devulcanization and compatibility enhancement.

TABLE 7 Nomenclature for Equations 7–15.

Symbol	Definition	Units
G'	Storage modulus	kPa
G^*	Complex shear modulus	kPa
δ	Phase angle	°
ω	Angular frequency	rad/s
m	Slope of the logG' versus log f fitting line	-
α	VECD model parameter derived from frequency sweep	-
C	Pseudo stiffness (ratio of current to initial complex modulus)	-
C_0	Initial pseudo stiffness (≈1.0)	-
t	Time	s
γ	Shear strain	-
γ_0	Applied strain amplitude in LAS test	-
A, B	VECD model fitting parameters for fatigue life prediction	-
N_f	Fatigue life (number of cycles to failure)	Cycles
γ_{max}	Maximum shear strain in pavement structure	-

2.1.4 Aggregates and mineral powder

The aggregates used in this study were diorite, and the mineral powder was limestone powder. Their basic properties are shown in Tables 3, 4 below.

2.2 Controlled devulcanization process

2.2.1 Influence of processing parameters on devulcanization degree

The preparation of devulcanized rubber-modified asphalt was carried out using a high-speed shear mixer (FLUKO FA25, Shanghai Fluid Mechanical Manufacturing Co., Ltd., China), with process parameters meticulously optimized to achieve an optimal balance between sufficient degradation of the rubber network and prevention of excessive asphalt aging. A FG-type dispersing head with a diameter of 25 mm was employed and positioned at approximately one-third of the depth from the bottom of the asphalt container. This configuration effectively prevented vortex

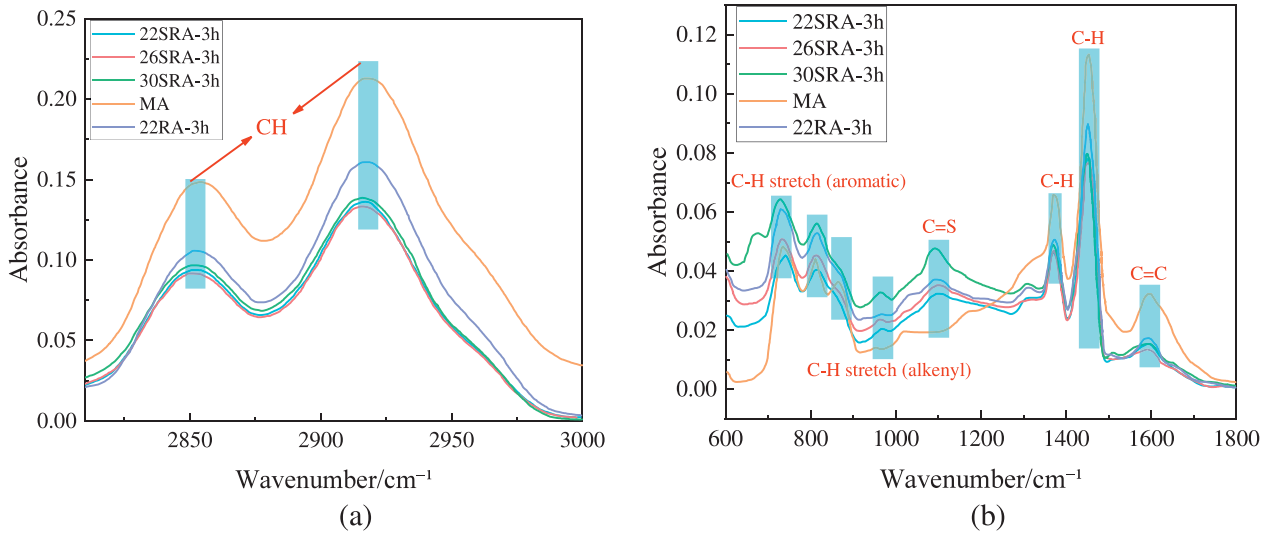

FIGURE 4
Comparison of absorption peaks in different asphalt spectra. **(a)** 2,800~3,000 cm^{-1}. **(b)** 600~1,800 cm^{-1}.

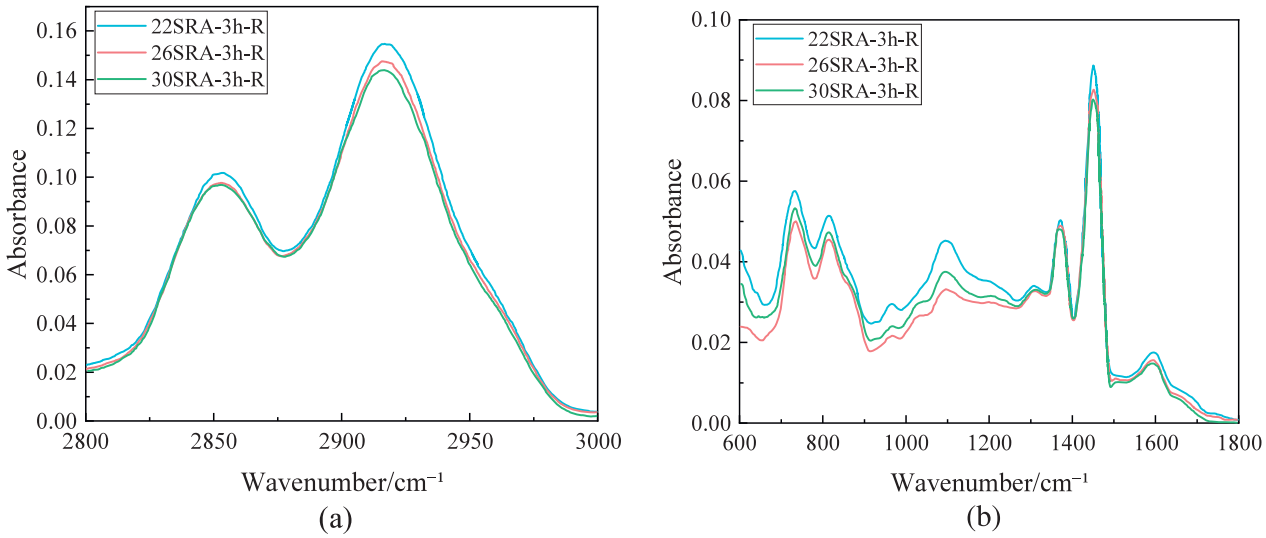

FIGURE 5
Comparison of absorption peaks in cracked high-content rubber asphalt spectra. **(a)** 2,800~3,000 cm^{-1}. **(b)** 600~1,800 cm^{-1}.

formation while ensuring uniform mixing throughout the volume. Based on the rotor diameter and operational rotational speed, the maximum shear rate in the system was calculated to be approximately 7,000 s^{-1}. Pretreatment: Precisely weighed CRM was preheated in a constant-temperature oven at 150 °C for 15 min to remove moisture and improve its wetting characteristics. The base asphalt was simultaneously heated to the target processing temperature. Mixing and Reaction: Once the base asphalt reached 160 °C ± 2 °C, the preheated CRM and the designated devulcanizing agent were introduced simultaneously. The CRM was introduced in two equal batches to ensure uniform dispersion and to mitigate a sudden surge in viscosity. An initial low shear rate of 800 ± 50 rpm was maintained for 20 min to achieve preliminary homogenization and wetting. Controlled Devulcanization: The system temperature was then elevated to and maintained at the optimal reaction temperature of 200 °C. This temperature and the subsequent reaction duration (1–6 h) constitute the critical controlled parameters for manipulating the extent of devulcanization. The reaction was then allowed to proceed for a predetermined duration. High-Intensity Shearing: Following the initial reaction period, once the granular texture of the CRM had largely disappeared, the shear rate was increased to 1800 ± 100 rpm for intensive mixing. This high-shear stage is crucial for final homogenization and for ensuring a uniform, micron-scale dispersion of the devulcanized rubber phases within the asphalt matrix. Throughout the entire process, temperature, rotational

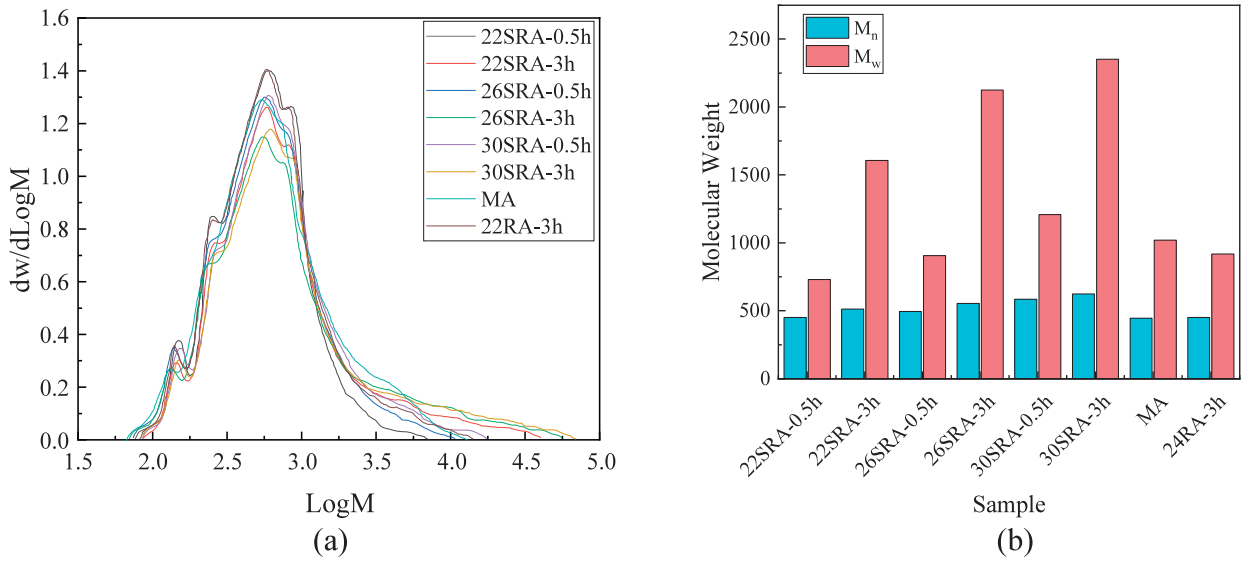

FIGURE 6
Evolution of molecular weight distribution in cracked rubber asphalt. **(a)** Molecular weight distribution comparison of different asphalts. **(b)** Molecular weight comparison of different asphalts.

speed, and time were strictly monitored to guarantee reliability and reproducibility.

2.2.2 Mixture preparation

This study conducted systematic research on the gradation design of rubberized asphalt (SRA) mixtures. Unlike conventional rubberized asphalt mixtures that typically use gap gradation, SRA mixtures employ a continuous dense-graded AC-13 formulation due to the higher degree of rubber powder cracking, which significantly reduces free asphalt content in the system. This selection is based on the following technical considerations: The cracking process effectively diminishes the rubber powder's adsorption effect on asphalt, ensuring more uniform asphalt distribution in the mixture and thereby addressing the compaction difficulties and volumetric instability issues caused by excessive free asphalt in conventional rubberized asphalt mixtures. The gradation design strictly adheres to the Technical Specifications for Construction of Highway Asphalt Pavements (JTG F40-2017), with detailed gradation curve parameters provided in Table 5. For determining the optimal asphalt-aggregate ratio, the Test Methods of Asphalt and Asphalt Mixtures for Highway Engineering (JTG E20-2011) was followed. Through a series of tests including Marshall testing, the optimal asphalt-aggregate ratios for various asphalt mixtures were ultimately determined, with specific data presented in Table 6.

2.3 Characterization methods

This study established a comprehensive material characterization system covering macroscopic performance tests and microscopic rheological analyses, as illustrated in Figure 1. By combining conventional indicators (such as penetration and softening point) with advanced testing methods (including dynamic shear rheometry and multiple stress creep recovery), and further integrating Fourier Transform Infrared (FTIR) spectroscopy. The study aims to systematically evaluate the fundamental characteristics and engineering performance of rubber-modified asphalt. For the mixtures, standard test methods including wheel tracking and low-temperature bending tests were employed to comprehensively examine their pavement performance. This multi-scale, multi-dimensional characterization approach not only meets specification requirements but also provides in-depth insights into the intrinsic properties of the materials, offering reliable evidence for process optimization and engineering applications. The specimens included base asphalt (MA), conventional rubber-modified asphalt (22RA-3h), and high-content devulcanized rubber asphalt in both unaged and aged conditions, enabling a comprehensive assessment of aging effects. The short-term aging was simulated using the Rolling Thin Film Oven Test (RTFOT) according to ASTM D2872, and the long-term aging was further simulated using the Pressure Aging Vessel (PAV) according to AASHTO R28. All specimens designated with the '-R′ suffix in this study have undergone this combined RTFOT and PAV aging procedure to represent the long-term aged condition.

2.3.1 Basic performance testing of asphalt

To characterize the fundamental properties of the asphalt binders, this study conducted standardized tests on samples with varying crumb rubber contents (22%, 26%, and 30% by weight of binder) and mixing durations (1.0, 2.0, and 3.0 h). First, penetration was measured using an automatic penetrometer under standard conditions (25 °C, 100 g load, 5 s duration) to directly assess the material's consistency. The softening point was determined using the ring-and-ball method at a constant heating rate of 5 °C/min; this value represents the temperature at which the asphalt softens sufficiently to allow a standard steel ball to penetrate, thereby providing a measure of its high-temperature performance. Ductility

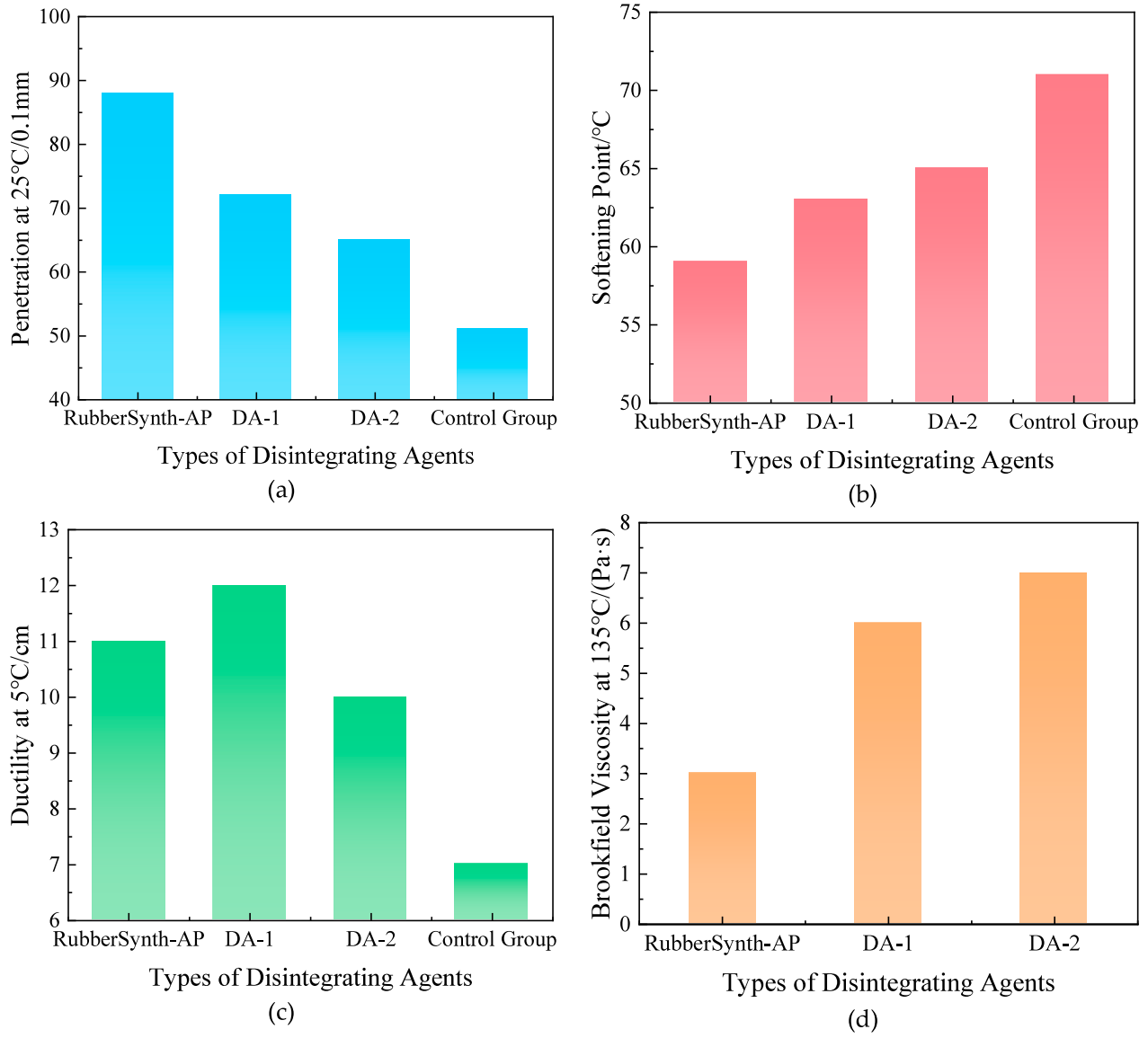

FIGURE 7
Conventional properties of rubberized asphalt with different devulcanizing agents at 22% crumb rubber content: **(a)** penetration at 25 °C; **(b)** softening point; **(c)** ductility at 5 °C; **(d)** Brookfield vis-cosity at 135 °C.

was measured using a ductilometer with the water bath maintained at 5.0 °C ± 0.1 °C and a constant stretching rate of 5 cm/min, characterizing the material's low-temperature deformation capacity. The Brookfield rotational viscosity was measured using a rotational viscometer at 135.0 °C ± 0.1 °C, as this is a critical parameter for assessing construction workability.

2.3.2 Rheological characterization

This study examined base asphalt (MA), conventional rubber-modified asphalt (22RA-3h), and devulcanized rubber-modified asphalt with varying mixing durations (1, 3, 4, and 6 h) and crumb rubber contents (22, 26, and 30 wt%). Multiple rheological characterization methods were systematically employed to evaluate the performance characteristics of each asphalt variant. The experimental protocol comprised four main components: (1) temperature sweep tests for temperature susceptibility evaluation; (2) Multiple Stress Creep Recovery (MSCR) tests for high-temperature rutting resistance assessment. For the MSCR test, specimens were prepared by placing the asphalt binder between parallel plates with a gap of 1.0 mm (for unaged and RTFOT-aged binders) as per standard protocol. For PAV-aged binders, which are stiffer, the binder was first heated to its pouring temperature without additional stirring (to avoid further aging or structural breakdown) and then directly used to prepare the dynamic shear rheometry specimen for testing. The specimens were not reconstituted to better simulate the actual aged condition in the field; (3) Linear Amplitude Sweep (LAS) tests for fatigue resistance characterization; and (4) frequency sweep (FS) tests for low-temperature performance analysis. This comprehensive test matrix was designed to not only evaluate fundamental asphalt performance parameters but

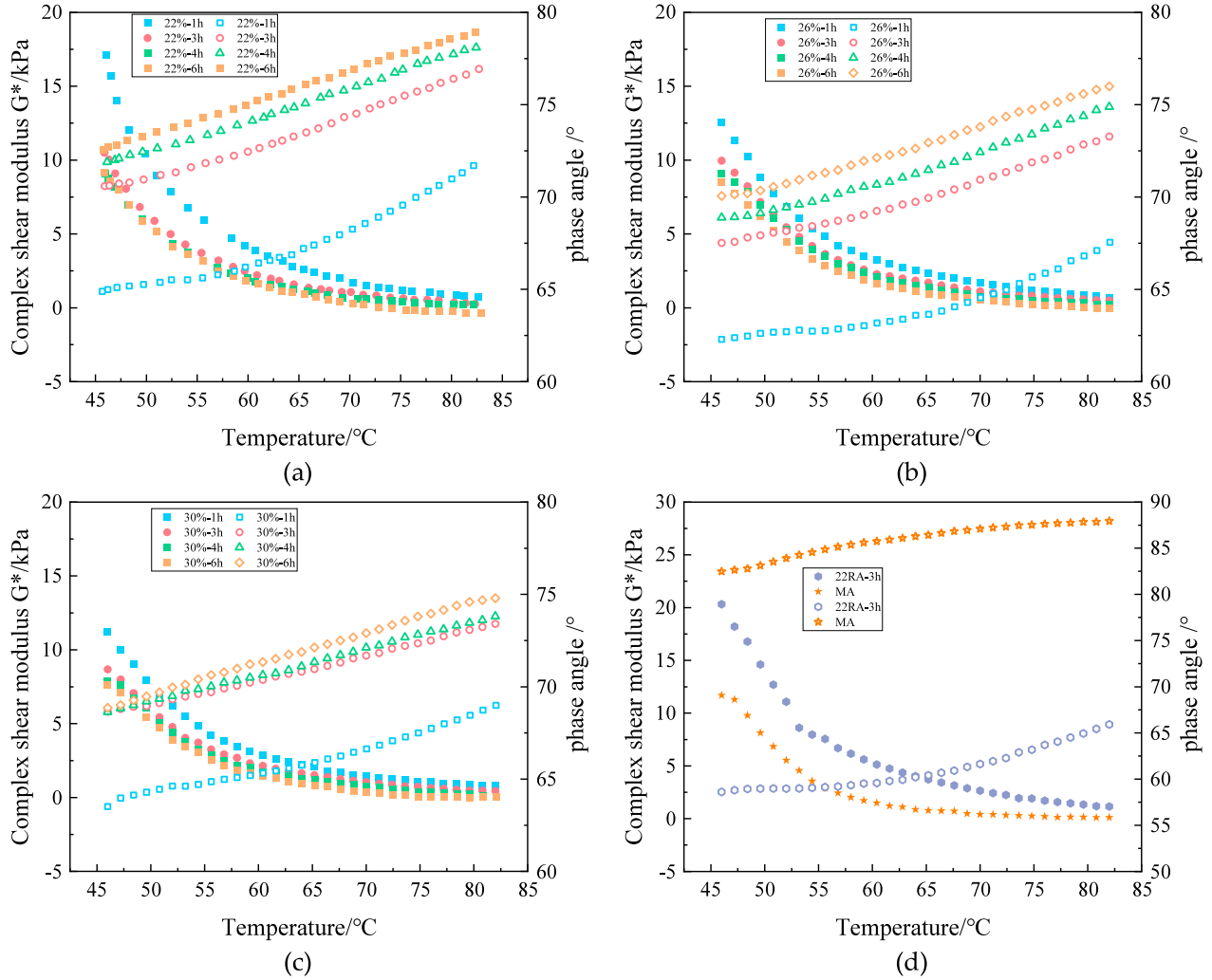

FIGURE 8
Complex modulus (G*) and phase angle (δ) versus CRM content: **(a)** 22%; **(b)** 26%; **(c)** 30%; **(d)** control.

also to elucidate the effects of devulcanization duration on the characteristics of rubber-modified asphalt.

2.3.2.1 High-temperature temperature sweep test

The temperature sweep tests were conducted using a dynamic shear rheometry in strain-controlled mode with a fixed strain of 10%. Particular attention was given to parallel plate gap selection, as the conventional 1 mm gap proved insufficient for accurate rheological characterization of high-content devulcanized rubber asphalt. Based on preliminary studies, a 2 mm gap was established as optimal for the 40-mesh crumb rubber, ensuring both data reproducibility and measurement validity by minimizing the phase angle while maximizing the rutting factor. The test parameters encompassed a temperature range of 58 °C–82 °C using 25 mm diameter parallel plates, with 10% strain and a loading frequency of 10 Hz. The measurements yielded critical rheological parameters, including the complex shear modulus (G), representing resistance to shear deformation; the phase angle (δ), indicating the stress-strain phase difference; the complex viscosity, describing temperature-dependent flow behavior; the failure temperature, defined as the critical temperature at which $G/sin\delta$ reaches 1.0 kPa; and the temperature susceptibility index (k), derived from the linear regression of $\log(G^*/sin\delta)$ versus temperature, whose absolute value quantitatively reflects the material's temperature sensitivity.

2.3.2.2 Multiple stress creep recovery (MSCR) test

The MSCR test was systematically conducted to evaluate high-temperature performance through a dual-stress protocol employing 0.1 kPa and 3.2 kPa stress levels. Each stress level consisted of 10 consecutive creep-recovery cycles (1 s loading followed by 9 s recovery), resulting in a total test duration of 200 s and thereby combining operational simplicity with testing efficiency. The test temperature was precisely maintained at 64 °C to align with both the base asphalt's failure temperature (65 °C) and its PG64 rating, ensuring consistent comparability

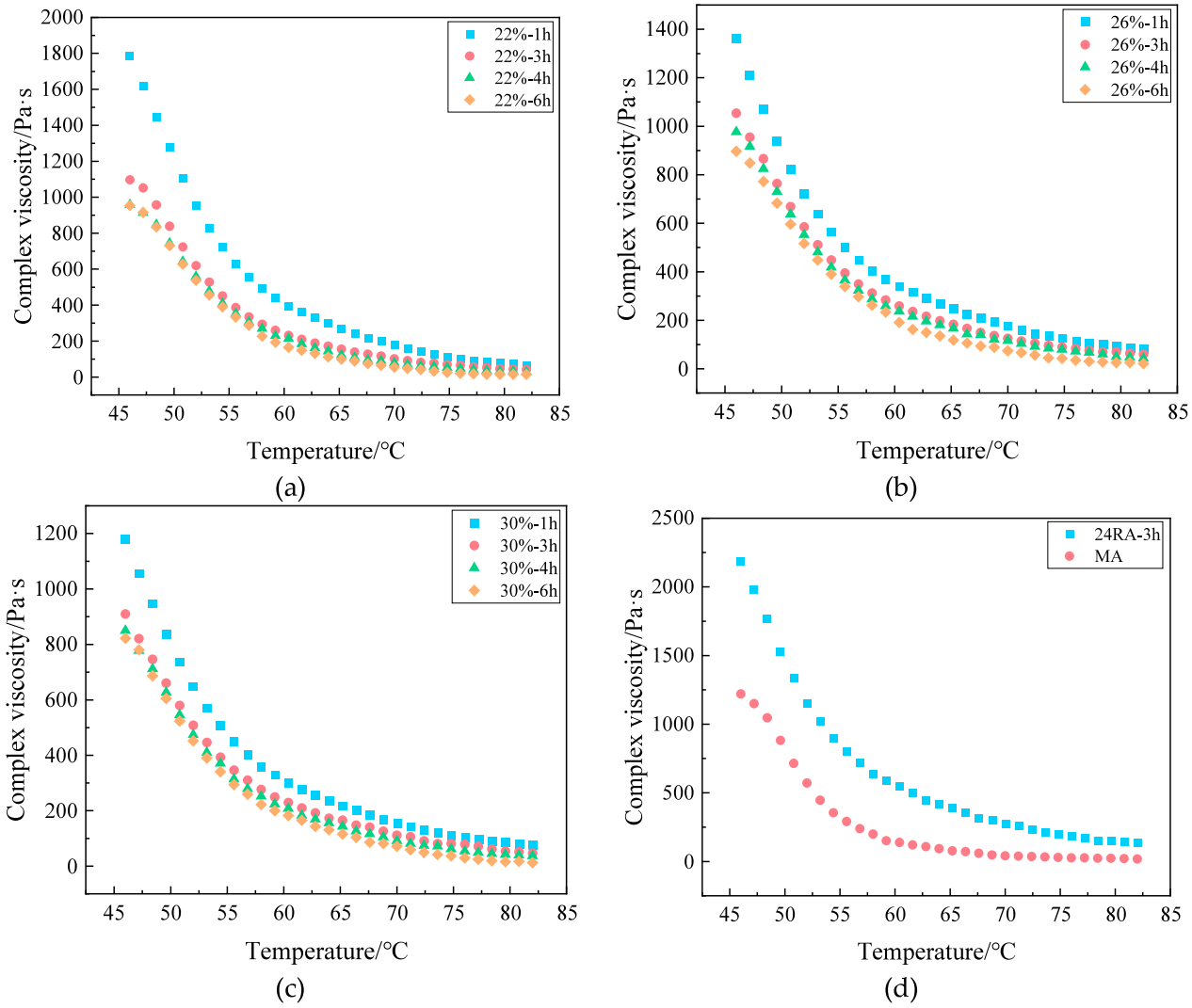

FIGURE 9
Variation curves of complex viscosity for different asphalt types. **(a)** Complex viscosity vs. temperature for 22% CRM samples at different mixing times. **(b)** Complex viscosity vs. temperature for 26% CRM samples at different mixing times. **(c)** Complex viscosity vs. temperature for 30% CRM samples at different mixing times. **(d)** Comparison of complex viscosity vs. temperature between 24RA-3h and MA samples.

across all test specimens. The specimens included base asphalt (MA), conventional rubber-modified asphalt (22RA-3h), and high-content devulcanized rubber asphalt in both unaged and aged conditions, enabling a comprehensive assessment of aging effects. As demonstrated in Figure 2, the characteristic creep recovery curves illustrate that asphalt materials develop peak strain upon loading, followed by partial strain recovery during the unloading phase. The progressive accumulation of non-recoverable strain exerts a cumulative influence on subsequent loading cycles.

The MSCR test employs three primary evaluation parameters to assess asphalt performance: the recovery rate (R), calculated through Equations 1 and 2, which quantifies the material's elastic deformation capability; the non-recoverable creep compliance (Jnr), determined by Equations 3 and 4, which characterizes the high-temperature deformation resistance; and the stress sensitivity parameters (R_{diff} and J_{nrdiff}), derived from Equations 5 and 6, which reveal the material's nonlinear characteristics.

$$R(100,N) = \frac{\gamma_p - \gamma_{nr}}{\gamma_p - \gamma_0} \times 100\% \quad (1)$$

$$R_{0.1} = \sum_{N=1}^{10} R(100,N)/10 \quad (2)$$

$$J_{nr}(100,N) = \frac{\gamma_{nr} - \gamma_0}{100} \quad (3)$$

$$J_{nr0.1} = \sum_{N=1}^{10} J_{nr}(100,N)/10 \quad (4)$$

$$R_{diff} = \frac{R_{0.1} - R_{3.2}}{R_{0.1}} \times 100\% \quad (5)$$

$$J_{nrdiff} = \frac{J_{nr3.2} - J_{nr0.1}}{J_{nr0.1}} \times 100\% \quad (6)$$

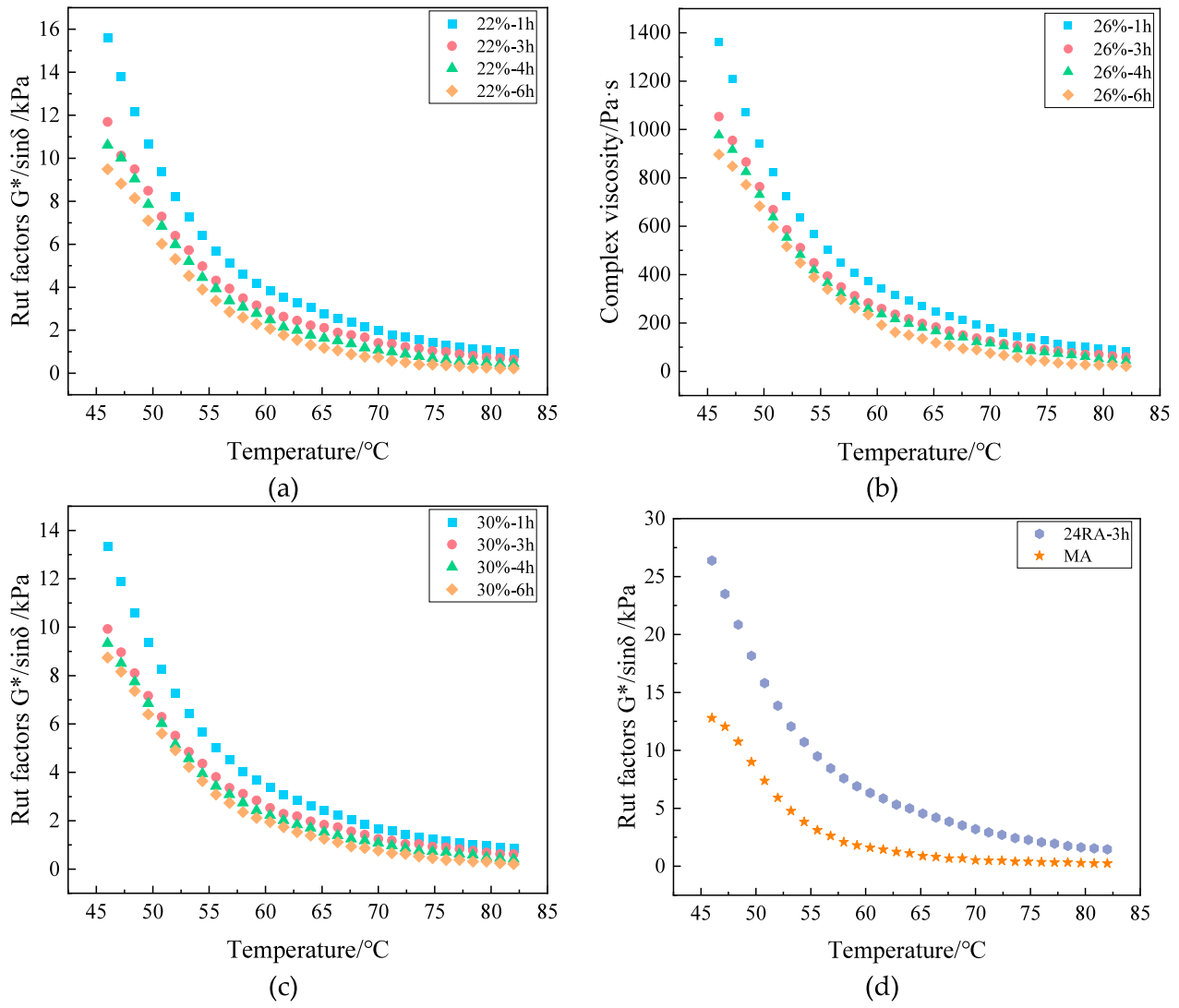

FIGURE 10
G*/sinδ variation curves for asphalt binders with different crumb rubber modifier (CRM) contents: **(a)** 22% CRM; **(b)** 26% CRM; **(c)** 30% CRM; **(d)** control (neat) asphalt.

Where: γ_{nr} denotes the residual deformation per loading cycle; γ_0 represents the initial strain per loading cycle; γ_p is the peak strain per loading cycle; N is the number of loading cycles ($1 \le N \le 10$); $R_{0.1}$ is the deformation recovery rate (%) at a stress level of 0.1 kPa, $R_{3.2}$ is the deformation recovery rate (%) at a stress level of 3.2 kPa, $J_{nr0.1}$ is the non-recoverable creep compliance (kPa^{-1}) at a stress level of 0.1 kPa, and $J_{nr3.2}$ is the non-recoverable creep compliance (kPa^{-1}) at a stress level of 3.2 kPa.

2.3.2.3 Linear amplitude sweep (LAS) test

The LAS test comprises two sequential stages: an initial frequency sweep followed by an amplitude sweep. In the frequency sweep stage, testing was performed at a fixed temperature using a constant 0.1% strain amplitude across a frequency range of 0.2–30 Hz. The subsequent amplitude sweep stage employed a fixed frequency of 10 Hz while linearly increasing the strain from 0.1% to 30% over a duration of 300 s. Through comprehensive analysis of the phase angle and shear stress versus strain relationships, this study confirmed the validity of the peak shear stress as a robust indicator of fatigue failure. This parameter not only effectively discriminates between the fatigue characteristics of base and modified asphalts but also maintains a strong correlation with fundamental elastic material properties.

The systematic examination of the evolution patterns of the phase angle and shear stress under strain enabled a critical evaluation of various fatigue failure criteria. As illustrated in Figure 3, the base asphalt displays a pronounced phase angle peak during loading, whereas the 22SRA-3h modified asphalt exhibits a continuous increase in the phase angle without peak formation. This fundamental behavioral difference indicates that while the phase angle peak may serve as a viable failure criterion for base asphalt, its utility for evaluating modified asphalt proves substantially limited. Complementary analysis of the shear stress versus strain relationships in Figure 3b reveals that both material

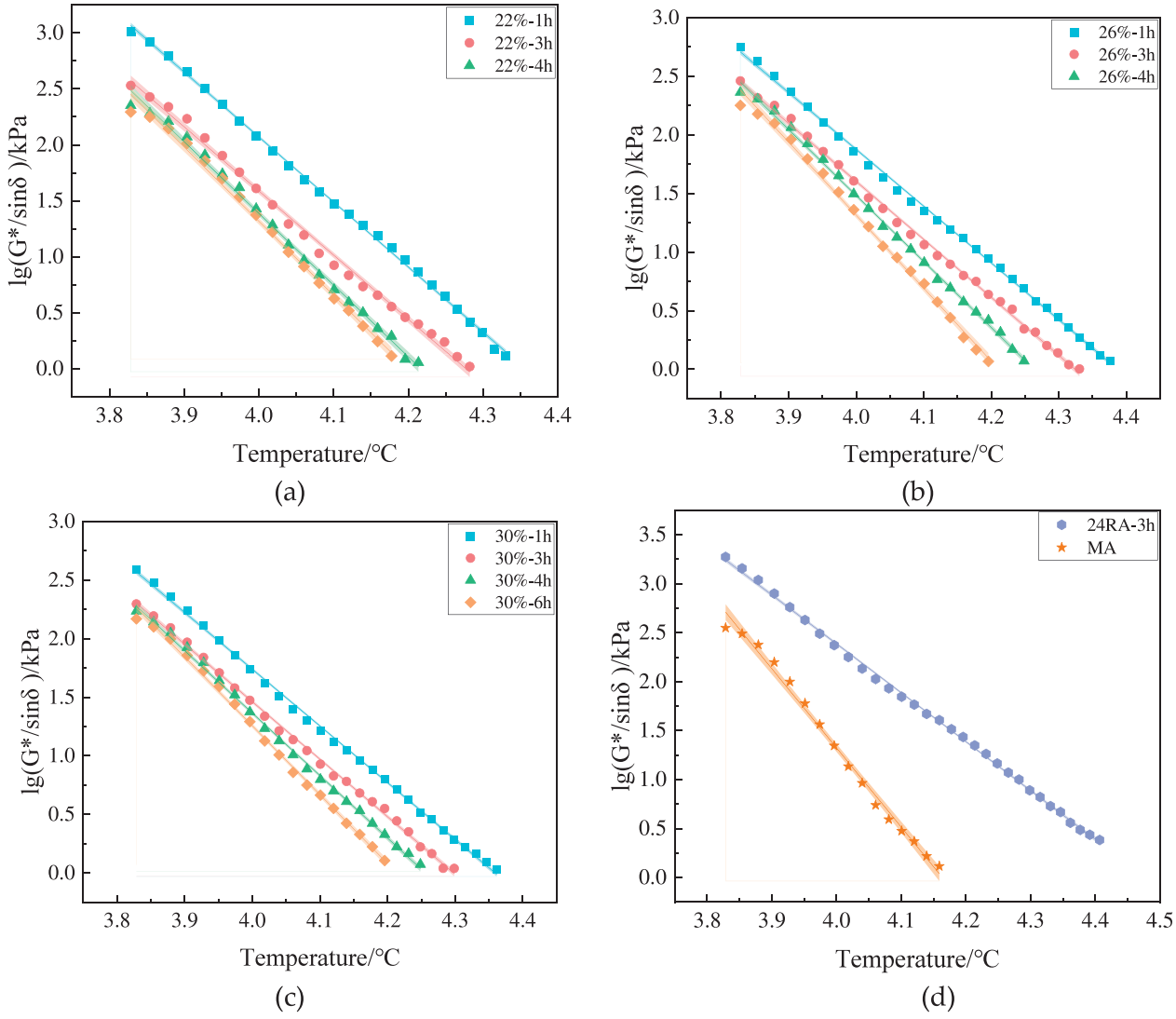

FIGURE 11
Fitting curves of rutting factor (G*/sinδ) for asphalt binders with different crumb rubber modifier (CRM) contents: **(a)** 22% CRM; **(b)** 26% CRM; **(c)** 30% CRM; **(d)** control asphalt.

types exhibit distinct peak shear stress characteristics. However, the base asphalt demonstrates earlier stress peaking at smaller yield strains, whereas the modified asphalt sustains higher stress levels to greater strains—behavior that correlates directly with its enhanced elastic performance. These findings collectively support the conclusion that the peak shear stress represents a more universally applicable parameter for characterizing the fatigue properties across diverse asphalt materials.

Following a rigorous assessment of the applicability and reliability metrics of all potential indicators, this study established the peak shear stress as the definitive fatigue failure criterion and developed an associated viscoelastic continuum damage (VECD) mechanics model for fatigue life prediction. This optimized selection achieves an ideal balance between the universality of the evaluation index and computational precision, thereby providing a robust technical framework for the comprehensive assessment of asphalt fatigue performance.

Building upon the theory of viscoelastic continuum damage (VECD) mechanics, this study developed a comprehensive fatigue life prediction framework for asphalt materials. The methodology derives essential material parameters through two sequential experimental phases: (1) frequency sweep testing to characterize the undamaged material through the determination of parameter α, followed by (2) linear amplitude sweep testing to quantify damage evolution data. The VECD model is then ultimately applied to calculate the fatigue life (N_f).

The frequency sweep phase involves the following standardized procedure for determining parameter α: The measured complex shear modulus (G^*) and phase angle (δ) are initially transformed into storage modulus (G') according to Equation 7; Following this, logarithmic fitting of G' versus frequency generates Equation 8; The material parameter α is then computed as $\alpha = 1 + 1/m$ from the slope (m) of the fitted curve.

TABLE 8 Linear fitting equations and goodness-of-fit indices for different asphalt binders.

Sample ID	Fitting equation: ln (G*/sinδ) = −klnT + b	R^2
22SRA-1h	ln(G*/sinδ) = −5.811 lnT +25.314	0.998
22SRA-3h	ln(G*/sinδ) = −5.733 lnT +24.520	0.999
22SRA-4h	ln(G*/sinδ) = −6.406 lnT +27.013	0.996
22SRA-5h	ln(G*/sinδ) = −6.626 lnT +27.820	0.999
26SRA-1h	ln(G*/sinδ) = −4.844 lnT +21.251	0.999
26SRA-3h	ln(G*/sinδ) = −4.945 lnT +21.394	0.998
26SRA-4h	ln(G*/sinδ) = −5.628 lnT +23.995	0.998
26SRA-5h	ln(G*/sinδ) = −6.226 lnT +26.217	0.998
30SRA-1h	ln(G*/sinδ) = −4.845 lnT +21.117	0.997
30SRA-3h	ln(G*/sinδ) = −4.912 lnT +21.109	0.999
30SRA-4h	ln(G*/sinδ) = −5.335 lnT +22.705	0.997
30SRA-5h	ln(G*/sinδ) = −5.880 lnT +24.776	0.999
MA	ln(G*/sinδ) = −8.088lnT +33.676	0.998
24RA-3h	ln(G*/sinδ) = −4.996 lnT +22.370	0.998

Regarding the linear amplitude sweep phase, in compliance with AASHTO TP101-14 standards and adopting Kim's method, the damage characteristic curve was developed through: 1) The material parameter α is computed as α = 1 + 1/m from the slope (m) of the fitted curve, representing the material's sensitivity to loading frequency. The damage characteristic curve was developed through quantification of cumulative fatigue damage (D) using Equation 9, wherein pseudo stiffness (C) was obtained from the ratio of complex shear modulus to initial modulus at discrete time intervals, representing the material's integrity degradation during fatigue loading; 2) Derivation of the fitting relationship between C and D (see Equation 10); 3) Development of the linear expression (Equation 11) via logarithmic transformation; 4) Integration of pseudo stiffness at peak shear stress (Equation 12) to determine model parameters A and B (per Equations 13 and 14). Subsequent substitution of these parameters into Equation 15 facilitates prediction of the asphalt material's fatigue life under specific strain levels, with γ_{max} denoting the maximum allowable shear strain in pavement structures. The definitions of the symbols used in Equations 7–15 are summarized in Table 7.

$$G'(\omega) = |G^*|(\omega) \times \cos\,\delta(\omega) \tag{7}$$

$$\log G'(\omega) = m(\log\,\omega) + b \tag{8}$$

$$D(t) \cong \sum_{i=1}^{N} \left[\pi\gamma_0^2(C_{i-1} - C_i)\right]^{\frac{\alpha}{1+\alpha}} (t_i - t_{i-1})^{\frac{1}{1+\alpha}} \tag{9}$$

$$C(t) = C_0 - C_1(D)^{C_2} \tag{10}$$

$$\log\left(C_0 - C(t)\right) = \log\left(C_1\right) + C_2 \cdot \log\left(D(t)\right) \tag{11}$$

$$D_f = \left(\frac{C_0 - C_{atPeakStress}}{C_1}\right)^{1/C_2} \tag{12}$$

$$A = \frac{f\left(D_f\right)^k}{k(\pi C_1 C_2)^\alpha} \tag{13}$$

$$B = 2\alpha \tag{14}$$

$$N_f = A\left(\gamma_{max}\right)^{-B} \tag{15}$$

2.3.2.4 Low-temperature frequency sweep test (FS)

Low-temperature thermal cracking in asphalt pavements exhibits a strong dependence on the inherent low-temperature performance of the asphalt binder. Studies demonstrate that the low-temperature characteristics of asphalt account for up to 80% of pavement crack formation, highlighting the enhancement of low-temperature resistance as a critical strategy for mitigating thermal cracking. A comparative analysis revealed that parameters derived from relaxation modulus master curves show a strong correlation (R = 0.85–0.95) with bending beam rheometer (BBR) test results. Building upon these findings, this study adopted low-temperature frequency sweep testing at a controlled temperature of −12 °C to maintain comparability across all asphalt samples. Through frequency sweep testing, key viscoelastic parameters—including the storage modulus (G') and loss modulus (G'')—were acquired. Christensen's modified model (Equation 7) was applied to transform the storage modulus master curves into relaxation modulus master curves, providing both high computational accuracy and broad acceptance in the field. Utilizing the relaxation modulus master curves, Equations 16 and 17 were employed to determine the 60-s relaxation modulus (G(60s)) and the relaxation rate (m-value), respectively, thereby establishing a reliable basis for a comprehensive low-temperature performance evaluation.

$$\lg G(60s) = ax^2 + bx + c|_{x=\log(60)=1.78} \tag{16}$$

$$m_r(60s) = 2ax + b|_{x=\lg(60)=1.78} \tag{17}$$

2.3.3 Performance testing of asphalt mixtures

This study implemented a multi-index evaluation system to comprehensively assess the pavement performance of stabilized rubber asphalt (SRA) mixtures, base asphalt (MA) mixtures, and conventional rubber asphalt (22RA-3h) mixtures. For high-temperature stability evaluation, standardized wheel tracking tests were performed on 300 mm × 300 mm × 50 mm specimens under a 0.7 MPa wheel load at 60 °C, with a loading rate of 42 ± 1 passes/min. The dynamic stability (DS) and the deformation rate served as the primary evaluation metrics.

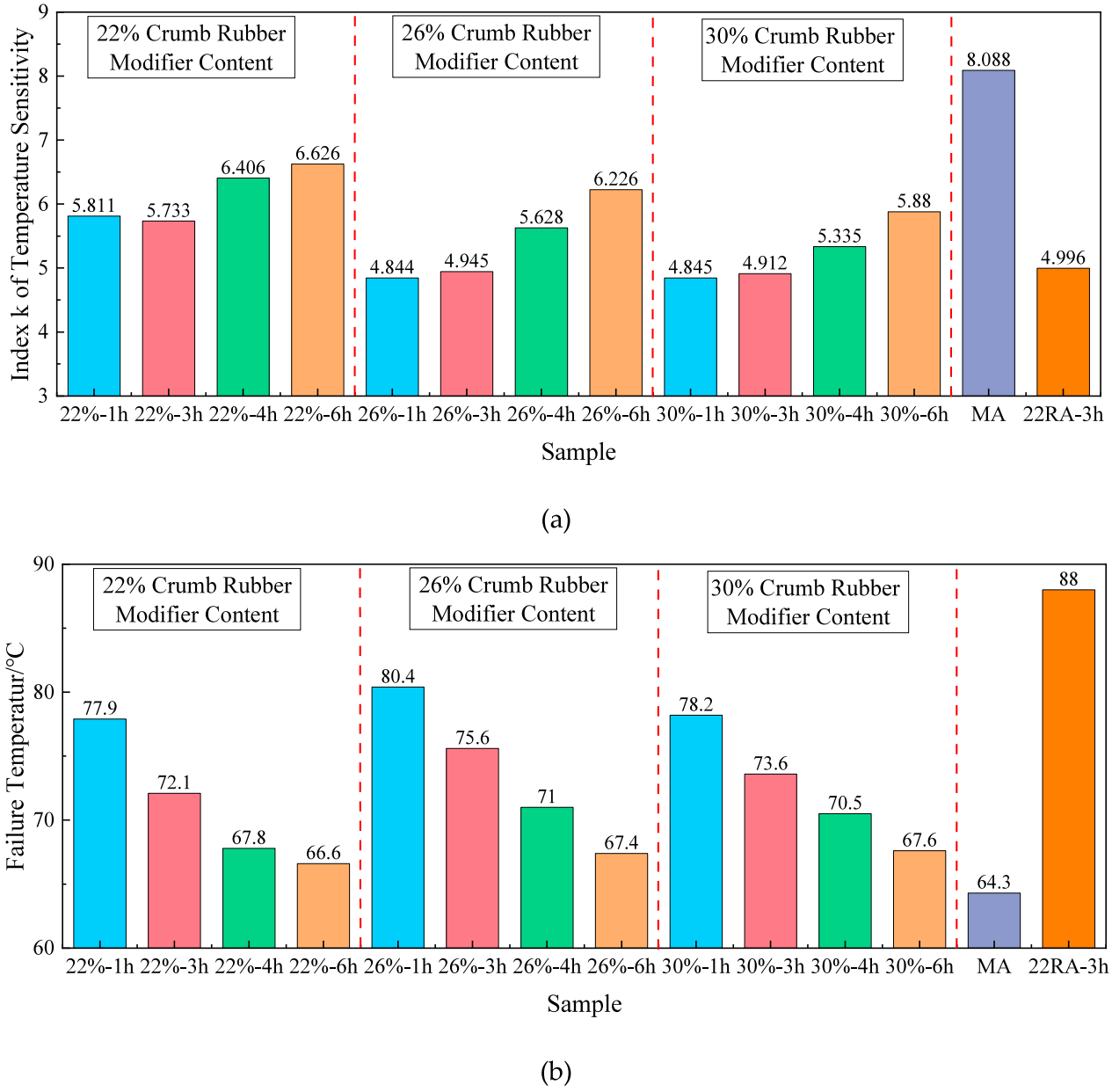

FIGURE 12
Variation characteristics of **(a)** temperature susceptibility index and **(b)** failure temperature for devulcanized rubber-modified asphalt.

Low-temperature crack resistance was characterized through three-point bending tests following stringent specimen preparation protocols: wheel-tracking slabs were first compacted and subsequently cut into standard beam specimens measuring 250 mm in length with a cross-section of 30 mm × 35 mm. Testing was conducted at −10 °C with a 200 mm span length and a loading rate of 50 mm/min to determine critical parameters, including the flexural tensile strength, flexural tensile strain, and bending stiffness modulus.

Water resistance assessment employed two complementary methodologies: (1) the immersion Marshall test evaluated performance variations after 30 min and 48 h soaking periods in a 60 °C water bath, with the retained stability as the key indicator; and (2) the freeze-thaw splitting test quantified moisture damage resistance through tensile strength ratio (TSR) comparisons before and after freeze-thaw cycles. This dual-method approach provides a robust evaluation of the mixture durability under wet conditions from multiple perspectives.

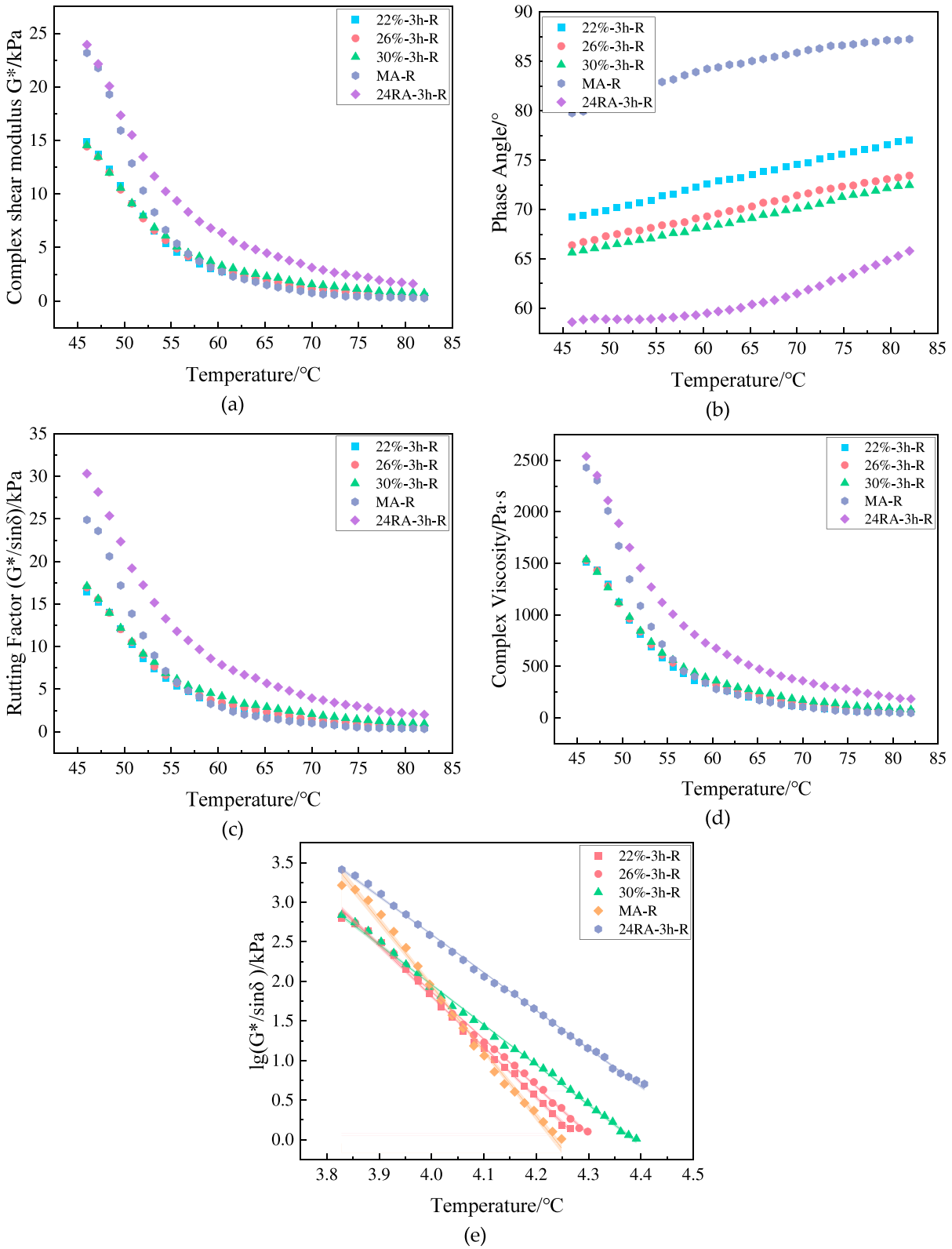

FIGURE 13
Comparison of viscoelastic parameters before and after aging: **(a)** complex shear modulus; **(b)** phase angle; **(c)** rutting factor; **(d)** complex viscosity; **(e)** complex shear modulus master curve.

TABLE 9 Summary of fitting equations and evaluation indices for rutting factor of different asphalts before and after aging.

Sample ID	Fitting equation: ln (G*/sinδ) = −klnT + b	R^2
22SRA-3h	ln(G*/sinδ) = −5.733 lnT +24.520	0.999
26SRA-3h	ln(G*/sinδ) = −4.945 lnT +21.394	0.998
30SRA-3h	ln(G*/sinδ) = −4.912 lnT +21.109	0.999
MA	ln(G*/sinδ) = −8.088lnT +33.676	0.998
22RA-3h	ln(G*/sinδ) = −4.996 lnT +22.370	0.998
22SRA-3h-R	ln(G*/sinδ) = −6.397 lnT +27.399	0.999
26SRA-3h-R	ln(G*/sinδ) = −5.997 lnT +25.859	0.999
30SRA-3h-R	ln(G*/sinδ) = −5.066 lnT +22.222	0.999
MA-R	ln(G*/sinδ) = −8.246 lnT +34.930	0.999
22RA-3h-R	ln(G*/sinδ) = −4.808 lnT +21.815	0.998

3 Results and discussion

3.1 Devulcanizer efficacy and mechanism

3.1.1 FTIR analysis of molecular structure evolution

To understand the devulcanization mechanism at the molecular level, Fourier Transform Infrared spectroscopy was performed on the asphalt materials, with the results presented in Figures 4–6. Comparative spectral analysis revealed several diagnostically important features (Figure 4): (1) the presence of C=S stretching vibrations at 1,110 cm^{-1} in rubber-modified asphalt, confirming the sulfur-rich nature of rubber components; (2) reduction of characteristic benzene ring vibration peaks from three in base asphalt to two in rubber asphalt, suggesting specific chemical transformations during modification; and (3) most notably, the appearance of a novel weak absorption at 970 cm^{-1} in devulcanized high-content rubber asphalt (SRA), attributed to trans-olefin = C-H out-of-plane bending vibrations.

This latter feature, absent in both base asphalt (MA) and conventional rubber asphalt (22RA-3h), provides direct evidence of molecular restructuring during controlled devulcanization. The formation of olefinic structures supports the proposed mechanism of selective cleavage of sulfur crosslinks, as the breakdown of the three-dimensional rubber network would generate such unsaturated bonds. The spectral evolution during different processing stages (Figure 5) further elucidates the chemical transformations: progressive attenuation of CH_2 symmetric/asymmetric stretching vibrations (3,000–2,800 cm^{-1}) coupled with intensification of olefinic characteristic bands (1,200–900 cm^{-1}) indicates consumption of saturated components and generation of olefin-rich degradation products through selective bond cleavage.

Complementary Gel Permeation Chromatography (GPC) analysis (Figure 6) revealed that devulcanized high-content rubber asphalt exhibits substantially elevated molecular weights (M_w reaching 1.4-2.0 times higher than conventional rubber asphalt), indicating integration of rubber-derived macromolecular fragments into the asphalt matrix. These molecular-level characterizations collectively provide evidence for the selective cleavage mechanism and the resulting microstructural evolution.

3.1.2 High-temperature rheological behavior: deciphering the network evolution

Figure 7 presents the conventional properties of the rubber-modified asphalt binders, each prepared with different devulcanizing agents at a fixed rubber content of 22%. The results demonstrate that the incorporation of a devulcanizing agent induces profound modifications in the material's properties. Critically, the RubberSynth-AP–modified binder exhibited the most pronounced changes, indicative of this agent's superior efficacy in disrupting the three-dimensional rubber network. This is evidenced by a 72.55% increase in penetration and a 16.90% reduction in softening point. The marked decrease in viscosity, coupled with enhanced penetration and ductility, confirms that RubberSynth-AP facilitates an optimal balance between the depth of devulcanization and the preservation of valuable elastic components. This optimal breakdown translates directly to superior workability without a catastrophic loss in high-temperature performance, a common pitfall of traditional devulcanizing agents. The observed performance hierarchy (RubberSynth-AP > DA-1 > DA-2) underscores the critical importance of molecular design in devulcanizing agents, for which selective cleavage and compatibility enhancement are paramount.

To quantitatively evaluate the devulcanization efficiency of RubberSynth-AP against commercial agents DA-1 and DA-2, the sol fraction of the crumb rubber was measured via toluene extraction according to ASTM D6814-02 after treatment under identical conditions. RubberSynth-AP yielded a significantly higher sol fraction of 82% ± 2%, compared to 65% ± 3% for DA-1 and 48% ± 4% for DA-2. This indicates a more effective breakdown of the crosslinked network. Concurrently, the viscosity-average molecular weight of the sol fraction reached 2.1×10^5 g/mol for the RubberSynth-AP-treated rubber, notably higher than the values of 1.5×10^5 g/mol and 0.9×10^5 g/mol obtained from DA-1 and DA-2, respectively. This inverse correlation between a higher sol fraction and a higher molecular weight strongly suggests a tendency for selective cleavage of crosslinks over random chain scission.

3.2 Rheology and microstructural evolution

3.2.1 High-temperature rheological behavior: deciphering the network evolution

The dynamic shear rheological tests unravel the effects of rubber content and devulcanization duration on the viscoelastic properties of SRA, as depicted in Figures 8–10. The observed monotonic decrease in complex modulus (G^*) and increase in phase angle (δ) with extended mixing time (at constant rubber content) provide

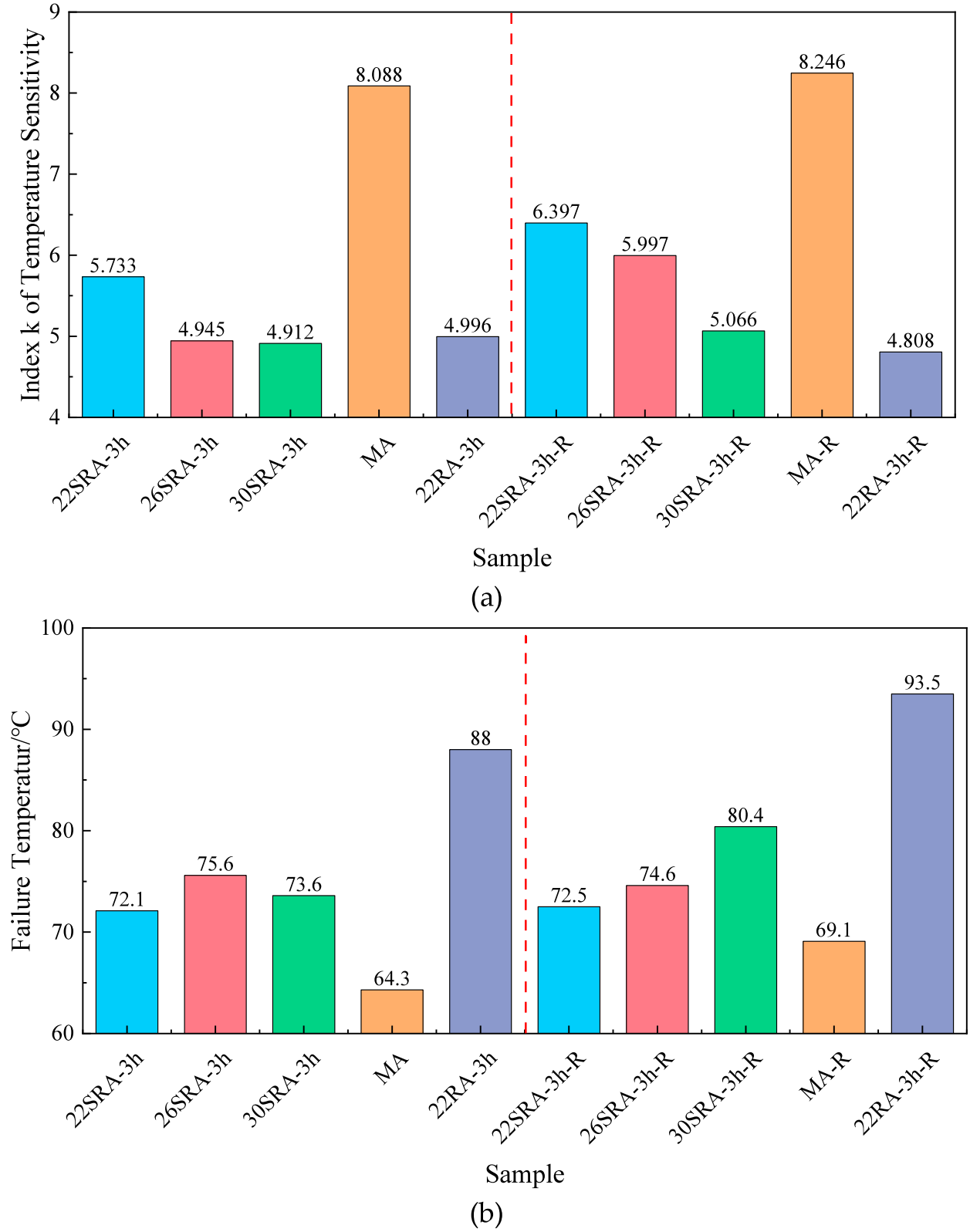

FIGURE 14
Variation characteristics of **(a)** temperature susceptibility index and **(b)** failure temperature for devulcanized rubber-modified asphalt after aging.

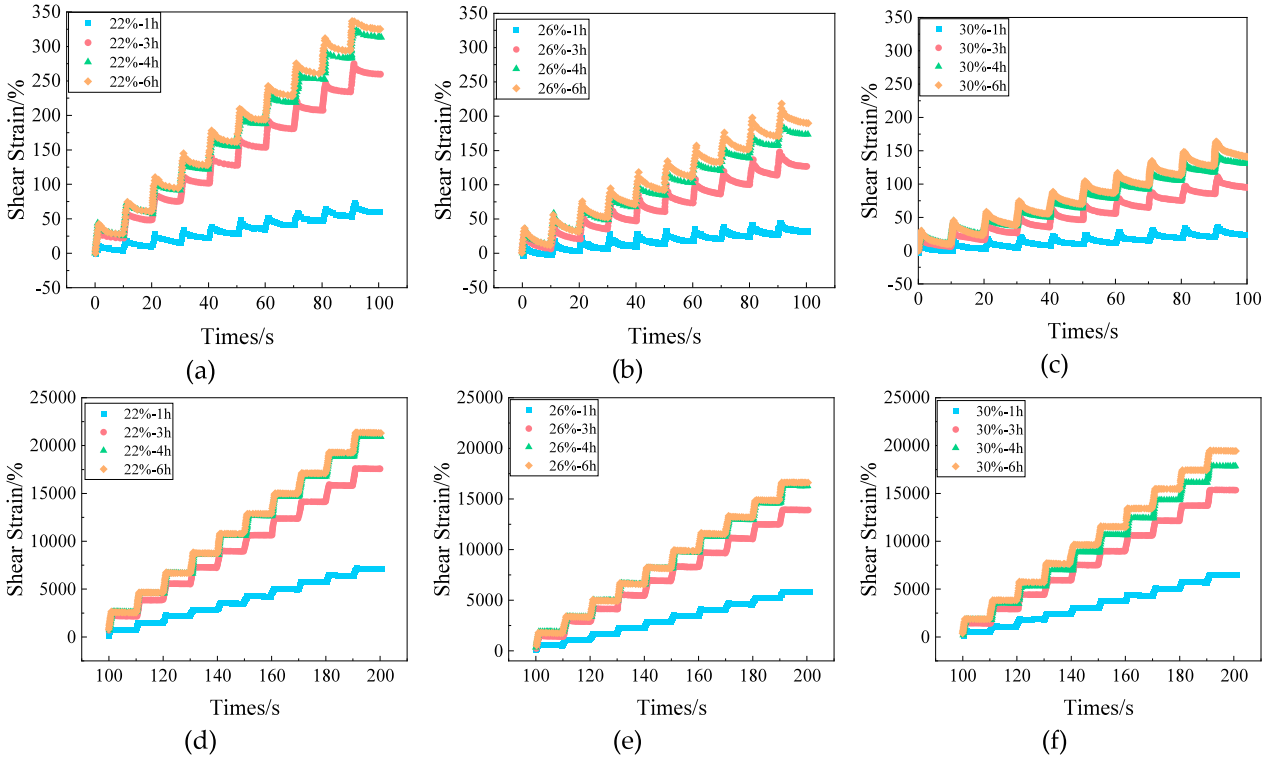

FIGURE 15
Cumulative strain-time curves under different stress levels and CRM contents: **(a)** 0.1 kPa, 22%; **(b)** 0.1 kPa, 26%; **(c)** 0.1 kPa, 30%; **(d)** 3.2 kPa, 22%; **(e)** 3.2 kPa, 26%; **(f)** 3.2 kPa, 30%.

direct evidence of the progressive dismantling of the elastic rubber network into viscous, asphalt-compatible fragments.

A pivotal finding was the convergence of key rheological parameters (G, δ, η, $G^*/sin\delta$) for the SRA binders with different initial rubber contents upon reaching stable devulcanization conditions (approximately 3–4 h). This convergence indicates that the final rheological behavior is less dependent on the initial rubber loading and is governed more by the ultimate state of the devulcanized rubber phase—namely, its molecular weight distribution, chemical nature, and dispersion quality within the asphalt matrix. The binder with 26% CRM consistently exhibited the most favorable set of high-temperature performance properties after optimal devulcanization. This outcome is attributed to an ideal residual content of partially devulcanized rubber particles that act as elastic nodes, forming a reinforcing "pseudo-network" within the softened asphalt matrix and thereby achieving an optimal synergy between elasticity and viscosity.

Data points exhibiting rutting factor ($G^*/\sin\delta$) values below 1.0 kPa were excluded prior to logarithmic transformation of the remaining dataset. Figure 11 presents the linear regression curves of $\ln(G^*/\sin\delta)$ as a function of temperature. Table 8 and Figure 12 summarize the functional relationships and evaluation parameters derived from linear regression analysis of rutting factor versus temperature in semi-logarithmic coordinates for different asphalt formulations.

The failure temperature and the temperature susceptibility index (k), both derived from the rutting factor (see Figure 11; Table 8), further corroborate the proposed network evolution. The monotonic increase in the k-value with extended devulcanization time signifies a heightened sensitivity to temperature fluctuations, which is a direct consequence of the diminishing elastic rubber network. Conversely, the observed inverse correlation between rubber content and the k-value at fixed reaction durations highlights the role of residual rubber components in stabilizing the system's response to thermal changes. The binders with 26% and 30% CRM demonstrated superior failure temperatures, with the 26% formulation outperforming all others. This result again underscores the existence of an optimal formulation window for achieving the best performance trade-off.

Figure 13 illustrates the evolution of the viscoelastic parameters for the asphalt materials before and after aging. As evidenced by the data, aging profoundly alters the material's viscoelasticity, manifesting as an elevated complex shear modulus and a reduced phase angle across all specimens. This behavior indicates that the aging process concurrently enhances high-temperature deformation resistance while compromising the material's elastic recovery capability. Table 9 and Figure 14 reveal that the devulcanized high-content rubber asphalt (SRA) exhibits distinctive performance attributes compared to other asphalt variants. The post-aging parameter variations for SRA are intermediate between those of the base and conventional rubber asphalts, preserving an

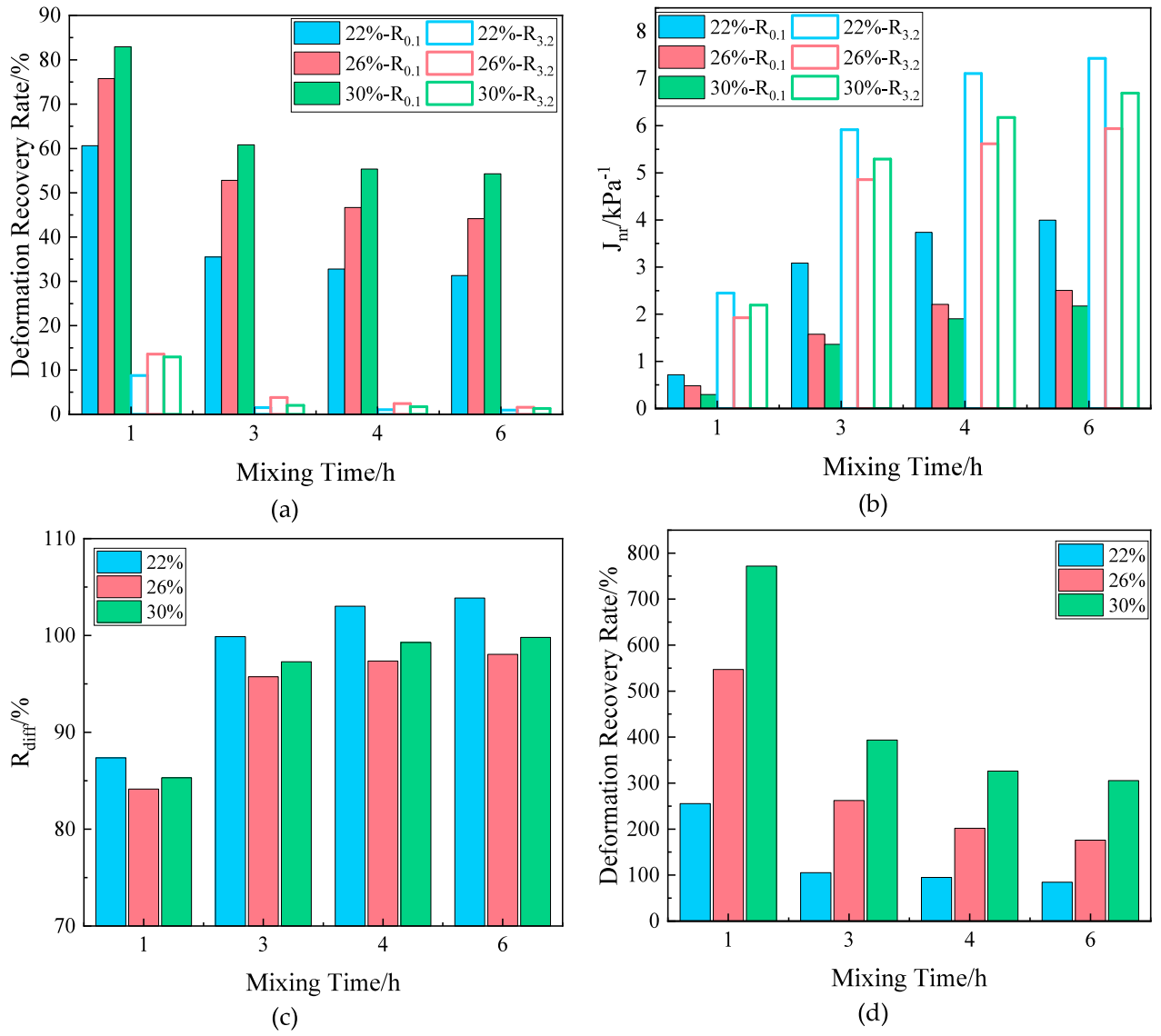

FIGURE 16
Variation of MSCR evaluation indices: **(a)** recovery rate; **(b)** non-recoverable creep compliance; **(c)** difference in recovery; **(d)** difference in Jnr.

optimal viscoelastic equilibrium. Quantitative analysis indicates that the SRA specimens demonstrate: a greater increase in the temperature susceptibility index than conventional rubber asphalt, yet a smaller increase than the base asphalt, while sustaining superior failure temperatures. The comparative evaluation identifies the specimen with 26 wt% rubber content as exhibiting the optimal overall performance. This formulation maintains excellent post-aging temperature stability, coupled with exceptional high-temperature rutting resistance. The experimental findings validate the exceptional suitability of this material for high-temperature engineering applications. These superior properties are directly correlated with the material's distinctive composition and microstructure, which enables a balanced evolution of performance during aging. Collectively, these results offer critical guidance for the selection and implementation of rubber asphalt materials.

3.2.2 Probing nonlinear viscoelasticity and stress sensitivity via MSCR

The Multiple Stress Creep and Recovery (MSCR) test results (see Figures 15 and 16; Table 10) provide profound insights into the nonlinear viscoelastic response and stress dependence of the SRA binders. The superior recovery rate (R) and lower non-recoverable creep compliance (J_{nr}) of the 26SRA-3h sample, particularly at the lower stress level of 0.1 kPa, signify a robust elastic response and exceptional resistance to permanent deformation. This behavior represents the macroscopic manifestation of the effective pseudo-network formed by the optimally devulcanized rubber.

The stress sensitivity indices (R_{diff} and $J_{nr,diff}$) are arguably the most indicative metrics. Their high values indicate a strong dependence of the material's rheological behavior on the applied stress level. The 26SRA-3h sample exhibited a more favorable

TABLE 10 Comparison of MSCR test evaluation indices for different asphalt binders before and after aging.

Sample ID	$R_{0.1}$ (%)	$R_{3.2}$ (%)	$J_{nr0.1}$ (kPa-1)	$J_{nr3.2}$ (kPa-1)	R_{diff} (%)	J_{nrdiff} (%)
22SRA-3h	32.48	0.051	2.745	5.562	99.92	103.05
26SRA-3h	53.12	2.28	1.268	4.478	95.68	253.42
30SRA-3h	59.88	1.72	1.042	4.952	97.21	376.83
MA	1.56	0.021	6.305	8.402	77.55	33.31
22RA-3h	78.92	22.9	0.175	0.982	71.18	461.07
22SRA-3h-R	44.68	3.17	1.664	3.248	92.97	95.33
26SRA-3h-R	55.25	6.43	0.894	2.782	88.41	210.63
30SRA-3h-R	67.49	8.67	0.54	2.42	87.19	348.37
MA-R	3.2	0.44	4.867	5.392	613.4	10.87
22RA-3h-R	82.49	33.96	0.12	0.604	58.88	404.59

balance—demonstrating a lower $J_{nr,diff}$ value compared to 22RA-3h—which indicates that the controlled devulcanization process mitigated the extreme stress softening typically observed in conventional rubber asphalt, while still retaining a strong elastic character at low stress levels. This unique combination of properties is highly desirable for pavement binders, which must perform effectively under a wide range of traffic loading conditions.

3.2.3 Fatigue damage evolution: a ductile-brittle transition governed by devulcanization

The fatigue damage evolution was analyzed within the theoretical framework of Viscoelastic Continuum Damage (VECD) mechanics. This approach characterizes the irreversible degradation of material integrity under repeated loading by introducing an internal state variable, the damage parameter (D). The central concept of the VECD model is the damage characteristic curve, which describes the unique relationship between the damage level (D) and the corresponding material integrity, represented by the pseudo stiffness (C). The pseudo stiffness is defined as the ratio of the current complex modulus to the initial modulus ($\boldsymbol{C} = |\boldsymbol{G}^*| / |\boldsymbol{G}_0^*|$), serving as an indicator of the material's remaining load-carrying capacity, which decreases from 1 to 0 as damage accumulates.

The fundamental relationship between C and D is given by the power-law model (as presented in Equation 18; Section 2.3.2):

$$C(t) = C_0 - C_1(D)^{C_2} \tag{18}$$

where the parameters C_1 and C_2 are material-specific constants that define the shape of the damage characteristic curve. A higher value of C_2 typically indicates a material with greater damage tolerance, as the pseudo stiffness declines more gradually with increasing damage.

The accumulation of damage (D) per loading cycle is driven by the released pseudo strain energy, and its evolution is calculated based on the governing equation (Equation 9; Section 2.3.2). The model parameters, including the damage evolution rate parameter (α) from frequency sweep tests and the fitting constants ($\boldsymbol{C_1}$, $\boldsymbol{C_2}$) from the LAS test, are ultimately used to predict the fatigue life ($\boldsymbol{N_f}$) under a given strain amplitude ($\boldsymbol{\gamma_{max}}$) via the fatigue life prediction model (Equation 15; Section 2.3.2).

The fatigue behavior, characterized through Linear Amplitude Sweep (LAS) tests and analyzed using Viscoelastic Continuum Damage (VECD) theory (see Figure 17), reveals a paradigm shift in the damage tolerance mechanism of the rubberized asphalt engineered through controlled devulcanization. Critically, the results demonstrate that devulcanization time serves as a precise parameter for controlling the material's fatigue response. An extended devulcanization duration transforms the role of crumb rubber from a rigid, stress-concentrating filler into a soft, energy-dissipating phase, thereby fundamentally altering the damage evolution pathway. This transformation is evidenced by the systematic upward shift of the damage characteristic curves (see Figures 17a–c). This transition signifies the formation of a novel microstructure in which the homogenized devulcanized rubber phases impede micro-crack initiation through enhanced compatibility and crack-tip blunting—a state unattainable in conventional rubber asphalt (22RA-3h).

Furthermore, a non-monotonic relationship between rubber content and fatigue life was identified and explained—a finding of significant practical importance. Increasing the rubber content from 22% to 30% at a fixed duration compromises fatigue performance, as incomplete devulcanization leaves a percolating network of rigid particles that act as pathways for rapid crack propagation. This result reveals an optimal loading threshold beyond which the benefits of added rubber are negated by inadequate decrosslinking.

The principal achievement of this approach is embodied by the 22SRA-3h formulation. This formulation achieves a 2.5–3-fold enhancement in fatigue life (N_f) over its conventional counterpart (see Figure 18), thereby resolving the long-standing paradox whereby the enhanced elasticity from rubber modification was often offset by compromised fatigue durability resulting from

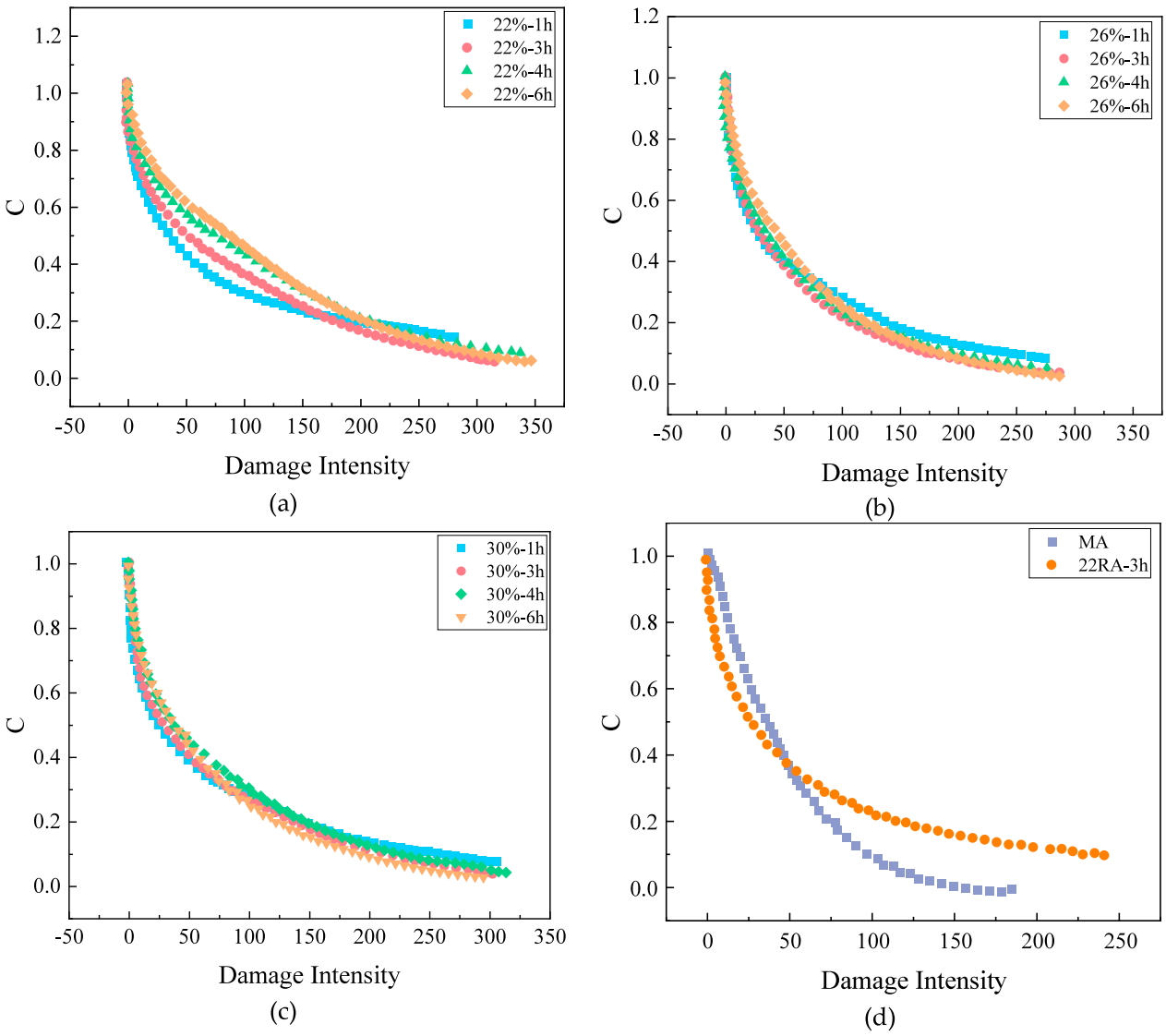

FIGURE 17
Fatigue damage characteristic curves with different CRM contents: **(a)** 22%; **(b)** 26%; **(c)** 30%; **(d)** control asphalt.

poor dispersion. The controlled process described herein decouples these typically competing properties, delivering both superior elasticity and exceptional damage tolerance.

Aging-triggered oxidative hardening universally shifts the damage characteristic curves leftward; however, the ranking of performance degradation reveals a critical durability crossover phenomenon (see Figure 19). The observed performance order—22SRA-3h > 26SRA-3h > 30SRA-3h > MA > 22RA-3h—is not arbitrary but is fully explicable through the lens of the devulcanization-governed microstructure model proposed herein.

The superior aging resistance of the conventional rubber asphalt (22RA-3h) is reinterpreted not as an inherent property but as a consequence of its intact, sacrificial rubber network, which shields the asphalt continuum from oxidation—a mechanism that was deliberately traded off in the present process to achieve initial performance gains. Conversely, the heightened aging susceptibility of the 22SRA-3h binder is framed as the other side of the same coin: its finely dispersed morphology and large interfacial area, which grant superb initial fatigue life, unintentionally create a high-density pathway for oxidative attack, thereby accelerating embrittlement.

This analysis identifies the 26SRA-3h sample as representing the quintessential optimized compromise. This formulation strikes an optimal balance by retaining a sufficient population of partially devulcanized, elastic domains to mitigate aging-induced brittle-ness, while simultaneously achieving a high degree of homogenization for exceptional initial performance. It successfully navigates the durability crossover, establishing it as the unequivocal choice for long-life pavement engineering.

3.2.4 Engineering low-temperature stress relaxation through controlled devulcanization

The low-temperature stress relaxation behavior, a critical indicator of thermal cracking resistance, was characterized through frequency sweep tests conducted at −12 °C (see Figures 20, 21).

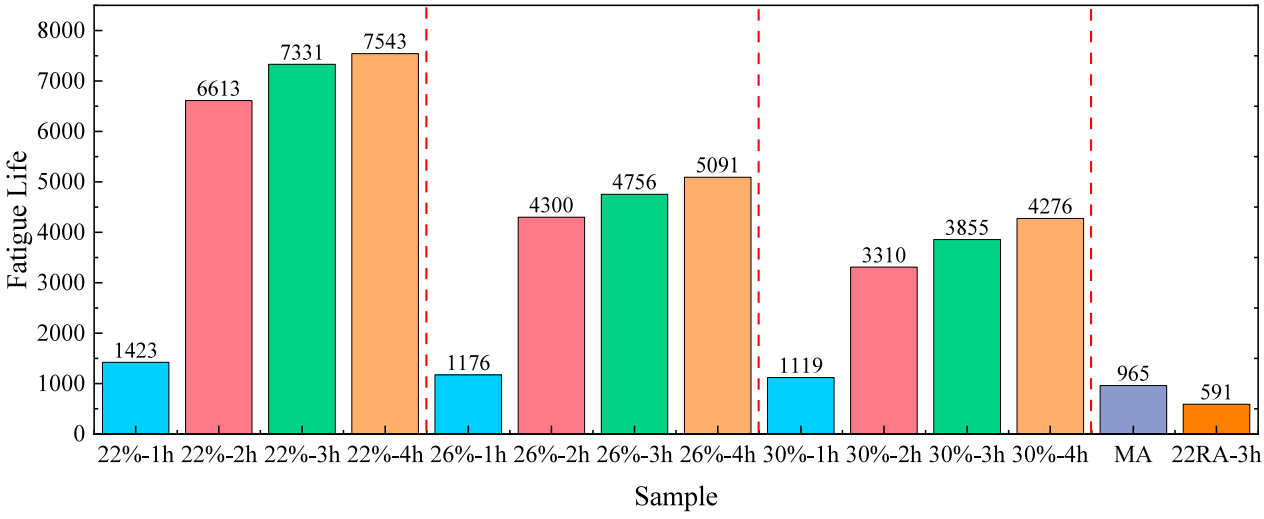

FIGURE 18
Fatigue life comparison of devulcanized rubber-modified asphalt under different conditions.

The results demonstrate that controlled devulcanization serves as a powerful tool for engineering the relaxation spectrum of asphalt binders.

Prolonged devulcanization time induces a pronounced softening effect and significantly enhances the stress relaxation capacity. This enhancement is quantitatively captured by a systematic reduction in the relaxation modulus (G(60s)) and a concurrent rise in the relaxation rate. This evolution provides direct evidence of the breakdown of the rigid, glassy rubber particles into flexible molecular chains that integrate into the asphalt matrix, thereby effectively plasticizing the binder and facilitating molecular mobility under cryo-genic conditions.

A key finding of this work is the identification of a distinct, two-stage evolution in the relaxation properties: 1) A rapid enhancement phase (0–3 h), during which the properties improve dramatically, exhibiting an approximately 40%–50% reduction in G(60s); 2) A subsequent stabilization plateau (>3 h), where further devulcanization yields diminishing returns. This biphasic kinetic behavior is a hallmark of a reaction-limited process approaching completion, thereby providing a critical scientific basis for optimizing industrial production parameters.

Furthermore, a non-intuitive structure-property relationship was established: although a higher rubber content yields the lowest modulus, it paradoxically exhibits an approximately 20% lower relaxation rate than the 22% content group. This finding indicates that excessive rubber loading, even after devulcanization, can marginally impede the viscous flow necessary for optimal stress dissipation. This nuanced understanding is vital for formulating high-performance binders tailored for extreme cold climates.

Aging invariably impairs low-temperature performance; however, this work uniquely quantifies the protective, antioxidant role of the residual rubber network. Following aging, all specimens exhibited an increased modulus and decreased relaxation rates (see Figure 22). However, the magnitude of this degradation was profoundly influenced by the initial formulation.

The specimen with 30% CRM exhibited exceptional aging resistance, showing only a 30%–40% reduction in its relaxation rate compared to a 70% reduction for the base asphalt. This order-of-magnitude difference in durability is attributed to two synergistic mechanisms inherent to the material system designed in this study: 1) Physical Shielding: The residual rubber particles act as flexible fillers that buffer thermal stress and constrain the volumetric contraction of the aged, hardened asphalt binder; Chemical Protection: The rubber phases contain inherent antioxidants and carbon black, which scavenge free radicals and retard the oxidative aging process, thereby effectively protecting the surrounding asphalt matrix.

This finding challenges the conventional view of rubber as a mere modifier, repositioning it as an active, multi-functional durability enhancer. The controlled devulcanization process enables the precise tuning of the dosage of this protective phase to achieve targeted longevity.

3.3 Pavement performance and benefits

The mixture performance results (see Figures 23–25) provide definitive validation that the enhancements engineered at the binder scale are successfully translated to the macroscopic composite level, fulfilling the promise of the multi-scale design approach.

3.3.1 High-temperature stability analysis

The rutting resistance results (see Figure 22) transcend mere performance reporting. The dynamic stability of the 26SRA-3h mixture represents a 305% improvement over that of the base asphalt mixture. More significantly, it validates the efficacy of employing a continuous dense-graded (AC-13) design for devulcanized rubber asphalt. The observed non-monotonic relationship between rubber content and dynamic stability is a direct consequence of the binder's rheology. The reduced viscosity and improved wettability of the SRA binder facilitate optimal coating of the aggregates and

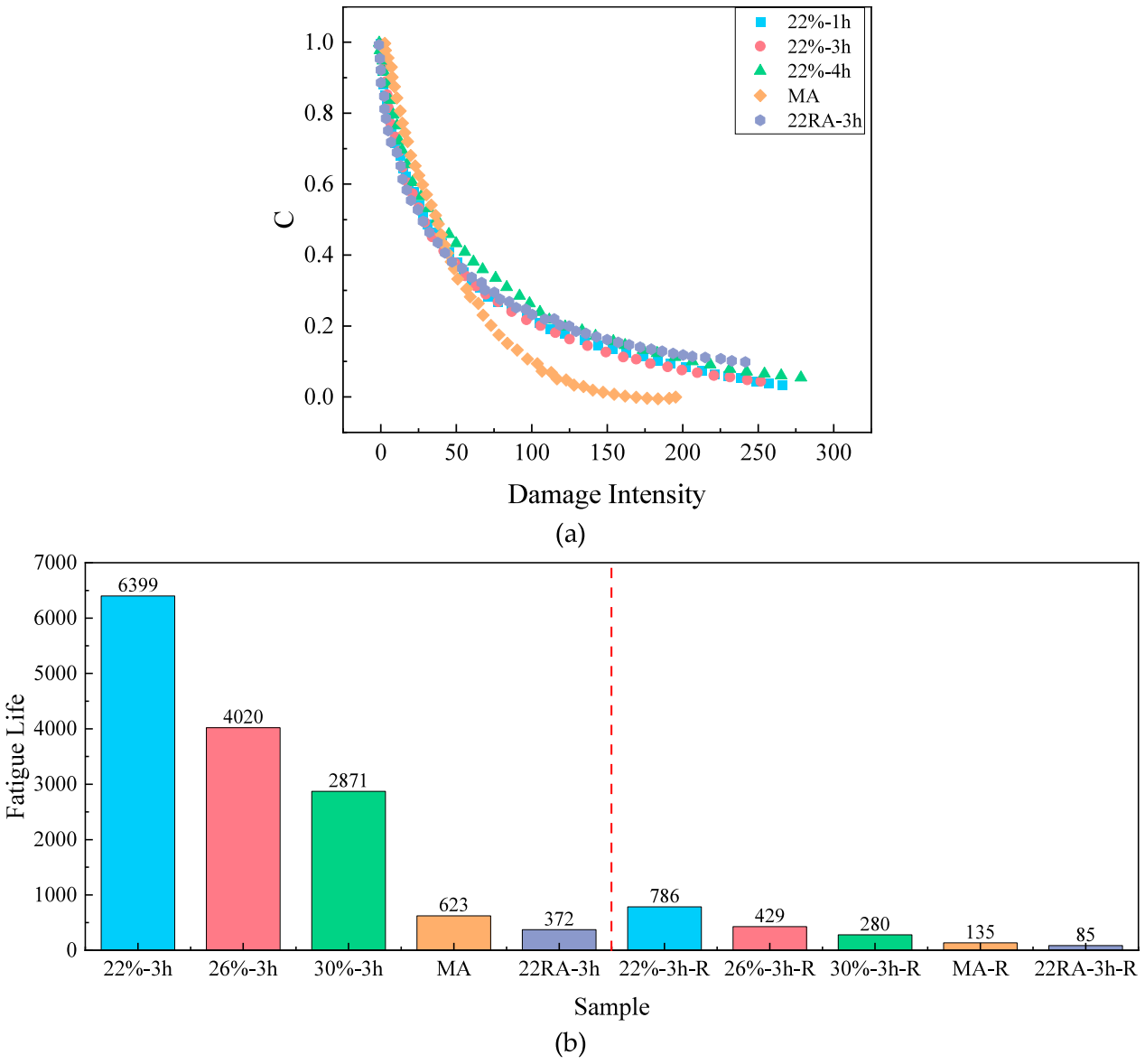

FIGURE 19
Effects of aging on fatigue characteristics: comparison of **(a)** damage curves and **(b)** fatigue life before and after aging.

promote denser packing, thereby enabling the formation of a strong mineral skeleton.

Conversely, the conventional rubber asphalt (22RA-3h) necessitates a gap-graded de-sign to accommodate its high viscosity, resulting in a less stable stone-on-stone structure that relies more heavily on the binder's intrinsic strength. This finding represents a fundamental shift in design philosophy: rutting resistance is enhanced not solely by strengthening the binder, but by enabling the creation of a superior aggregate skeleton—a more robust and sustainable mechanism.

3.3.2 Unlocked ductility and crack resistance at low temperatures

The low-temperature bending beam test results (see Figure 24) demonstrate a break-through in achieving superior ductility within a densely graded mixture—a combination traditionally considered paradoxical. The SRA mixtures exhibited a 50%–60% and 35%–45% increase in flexural strain over the MA and 22RA-3h mixtures, respectively.

This enhancement represents not a mere incremental improvement but a qualitative leap, stemming from the fundamental restructuring of the binder phase. The devulcanized rubber phases act as a distributed network of elastic, stress-absorbing domains within the asphalt mastic. This network effectively blunts microcrack initiation and arrests crack propagation through localized deformation and energy dissipation, thereby unlocking the intrinsic ductility of the composite, which is typically suppressed in conventional mixes by rigid particles or a brittle asphalt matrix.

The observed positive correlation between rubber content and flexural strain further confirms the role of the rubber phase as a

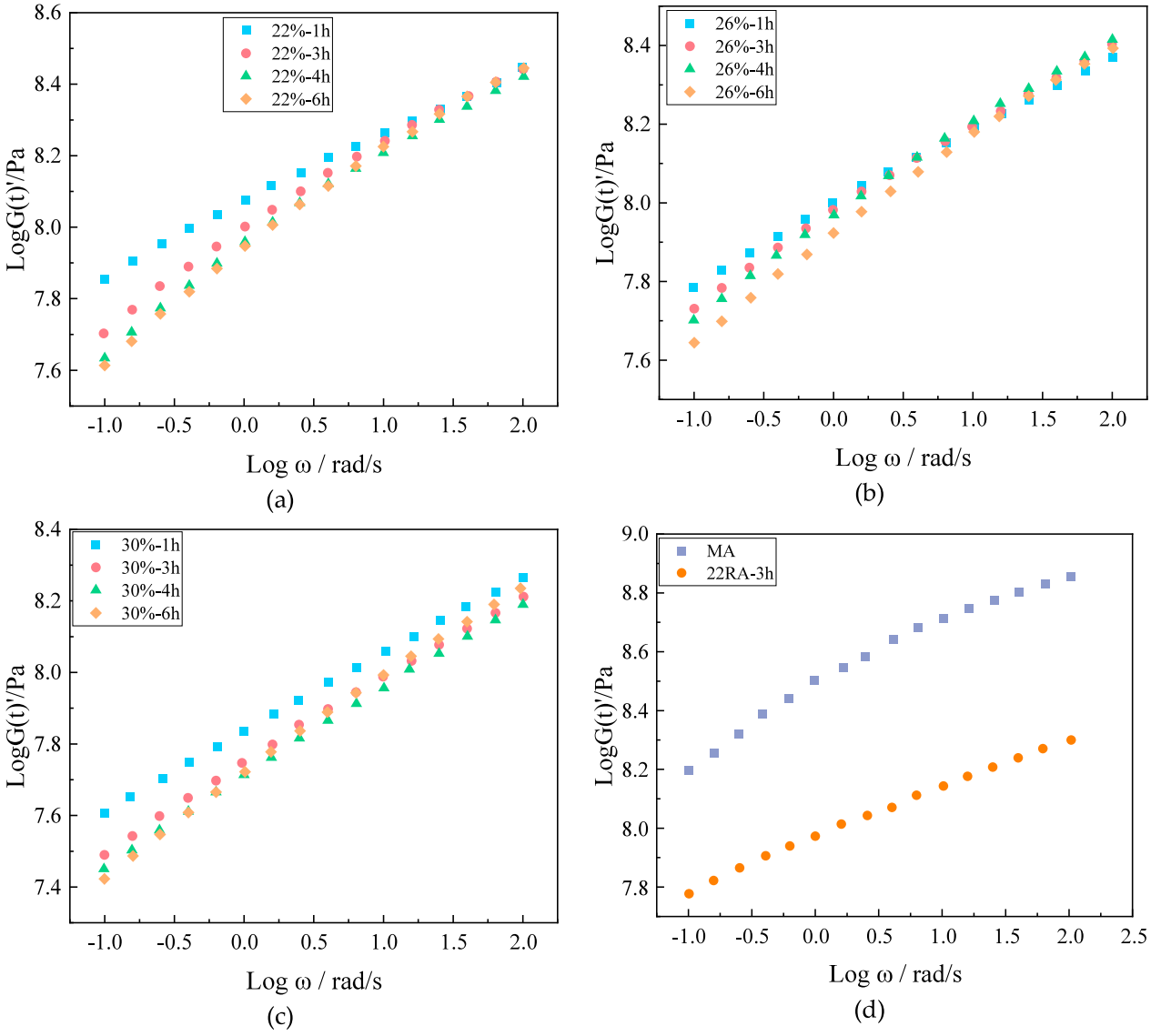

FIGURE 20
Storage modulus (G′) master curves for asphalt binders with different crumb rubber modifier (CRM) contents: **(a)** 22% CRM; **(b)** 26% CRM; **(c)** 30% CRM; **(d)** control asphalt.

primary driver of ductility. This finding establishes a new materials design principle: crack resistance can be systematically enhanced by engineering the volume fraction and morphology of a soft, elastic phase within a rigid composite—a concept validated herein for asphalt mixtures.

3.3.3 Moisture stability: balancing compatibility and hydrophilicity

The moisture stability results (see Figure 25) reveal a nuanced picture that under-scores the critical importance of interfacial chemistry. The SRA mixtures demonstrated a unique moisture resistance signature: their retained stability approximated that of the MA mixture but surpassed that of the 22RA-3h mixture.

The observed decrease in the moisture resistance indices with increasing rubber con-tent is a significant finding. The observed decrease in moisture resistance indices with increasing rubber content suggests a potential link between the devulcanization process and interfacial hydrophilicity. It is postulated that the process may generate polar molecules or expose functional groups that increase the susceptibility of the interface to water damage, even while enhancing compatibility in the asphalt phase. This correlation warrants further investigation through surface energy measurements to directly characterize the wettability of the modified binder-aggregate interface.

This insight is pivotal, as it moves the discussion beyond mere physical adhesion and into the realm of chemical interfacial engineering. This finding suggests that the future optimization of

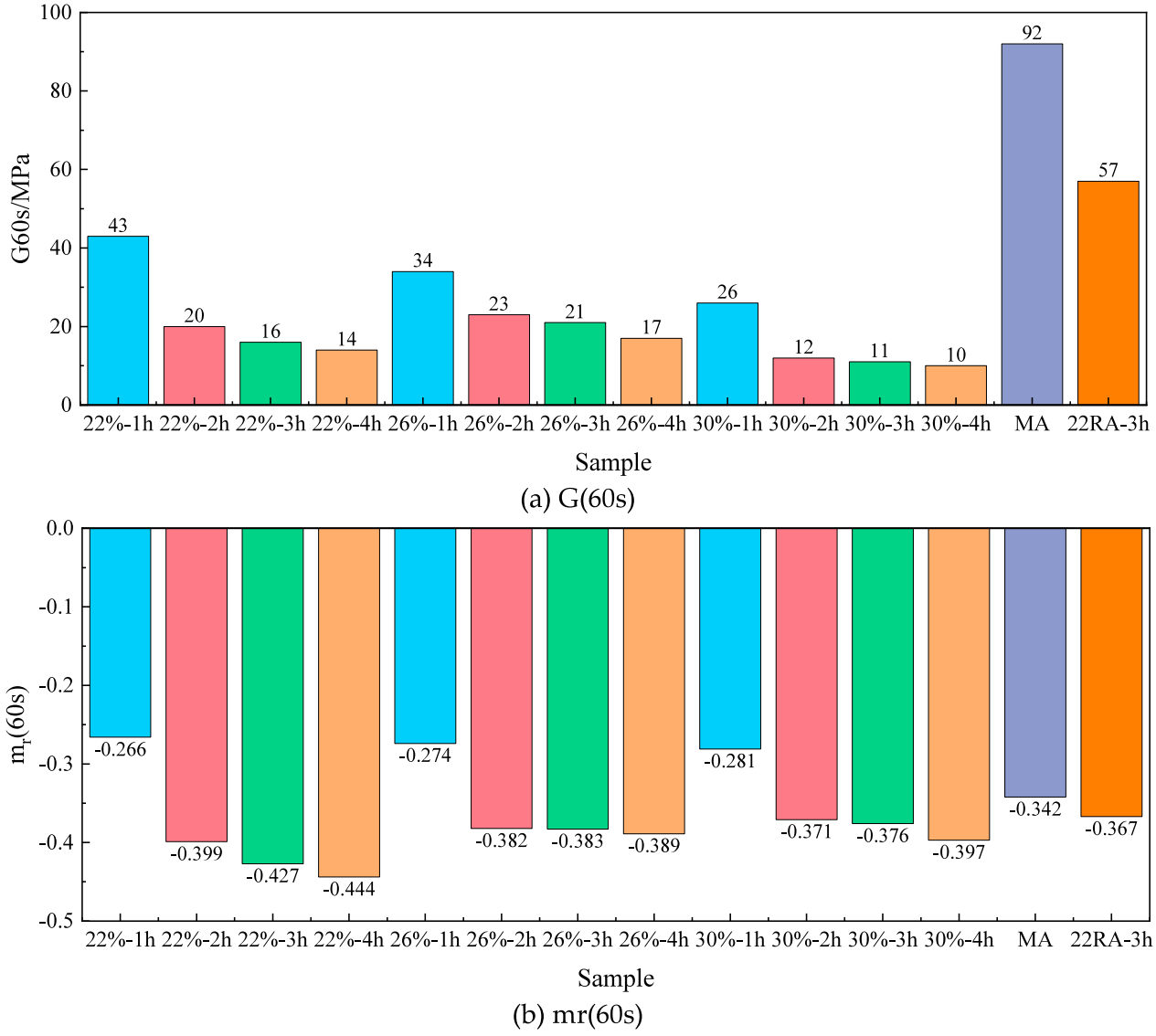

FIGURE 21
Comparison of **(a)** relaxation modulus [G(60s)] and **(b)** relaxation rate [m(60s)] for devulcanized rubber-modified asphalt.

devulcanizing agents should focus not only on network breakdown but also on passivating these newly generated polar sites to enhance hydrophobicity, thereby presenting a clear pathway for next-generation material design.

3.3.4 Life-cycle economic and environmental benefits

Life Cycle Cost Analysis (LCCA) is a widely adopted methodology for the economic evaluation of pavement systems. Rooted in economic theory, LCCA represents an operations research approach that identifies optimal investment strategies through the comparative analysis of alternative pavement life-cycle cost scenarios. Standard LCCA approaches encompass: (1) net present value (NPV), (2) annual cost, (3) rate of return, and (4) benefit-cost ratio analyses. A complete pavement LCCA integrates three benefit categories: direct economic, indirect economic, and environmental benefits. This investigation specifically examines the direct economic benefits of SRA asphalt pavement with respect to raw material costs.

The analysis considers three surface layer materials: the MA mixture, the 22RA-3h mixture, and the 26SRA-3h mixture. For a 1 km-long, 5 cm-thick dual-carriageway surface layer, the required mixture volume (V) was computed using Equation 19:

$$V = dhCL\rho \tag{19}$$

Where: V represents the mixture volume; d denotes the pavement width, which is taken as 7.5 m (calculated as 3.75 m × 2 for dual carriageways) in this study; h indicates the surface layer thickness, specified as 5 cm; C is the loose placement coefficient with a value of 1.20; L stands for the pavement length, set at 1 km for this analysis; and ρ signifies the density of the various asphalt mixtures.

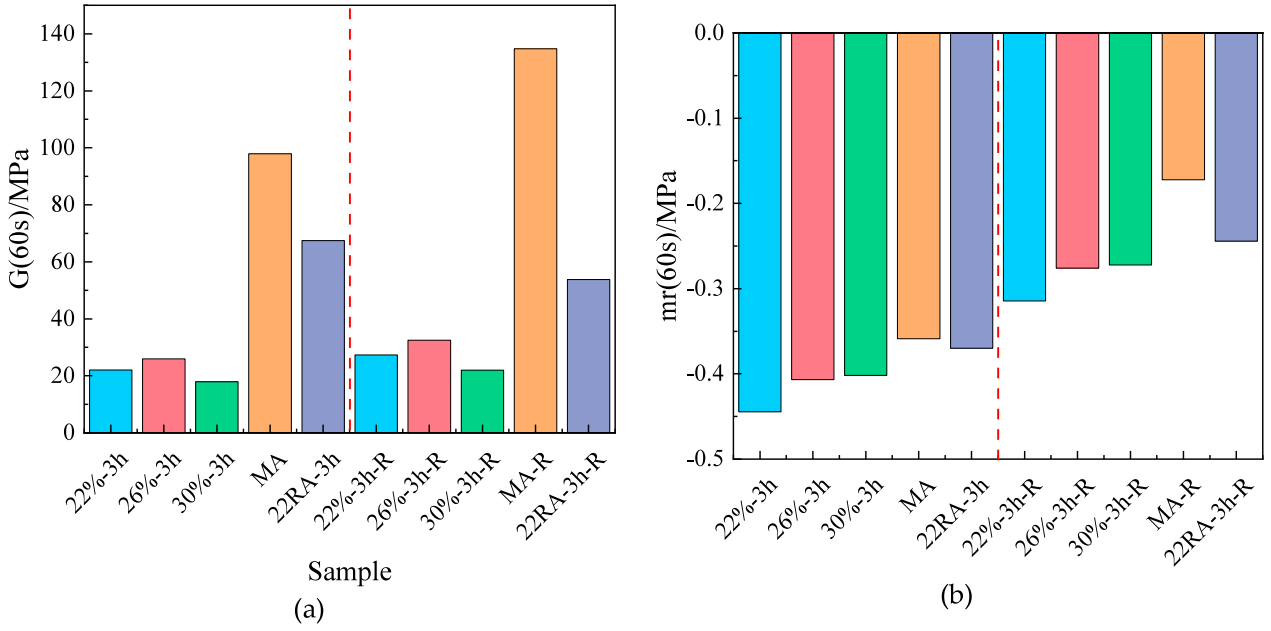

FIGURE 22
Low-temperature relaxation characteristics versus crumb rubber content: comparison of **(a)** relaxation modulus and **(b)** relaxation rate before and after aging.

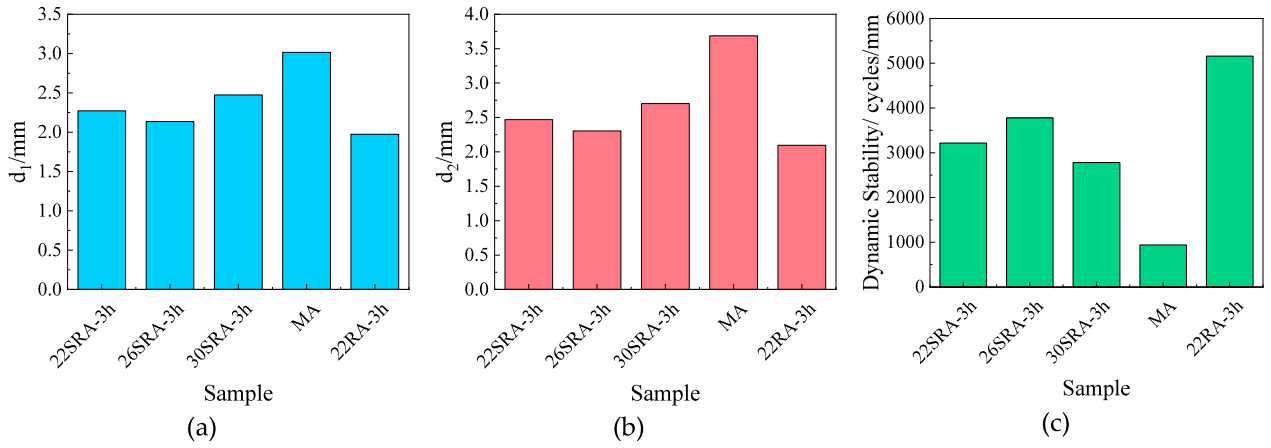

FIGURE 23
High-temperature stability test results: **(a)** deformation d_1; **(b)** deformation d_2; **(c)** dynamic sta-bility.

The unit material costs are provided in Table 11. The material consumption quantities and the corresponding costs for constructing a 1 km highway section using the different asphalt mixtures are presented in Table 12.

Table 11 demonstrates that constructing 1 km of 26SRA-3h mixture yields the lowest cost - ¥8,000 cheaper than MA mixture and ¥15,000 cheaper than 22RA-3h mixture. Therefore, using SRA mixtures for asphalt pavement construction not only reduces costs but also consumes substantial rubber powder (18 tons/km), alleviating environmental pressure while delivering significant economic and environmental benefits. This preliminary economic analysis considers only material cost savings. A comprehensive assessment including the energy consumption during the prolonged high-shear mixing process is necessary for full-scale engineering implementation.

3.4 Long-term aging performance and mechanistic analysis

To address the long-term durability of the developed binders, a comprehensive analysis was conducted on samples after RTFOT + PAV aging. The consolidated results, as presented in Figures 13,

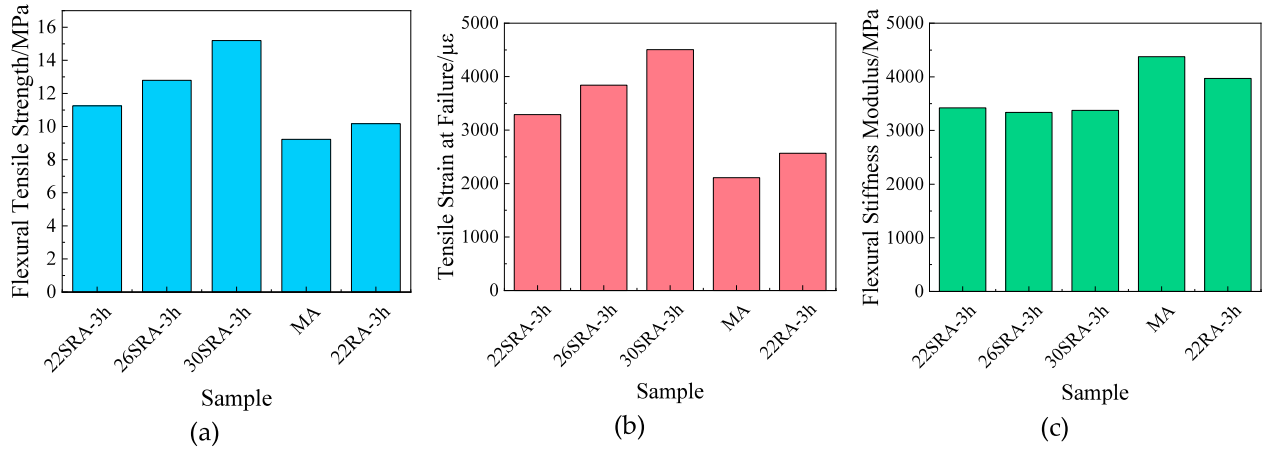

FIGURE 24
Low-temperature crack resistance test results: **(a)** flexural-tensile strength RB; **(b)** maximum bending strain εB; **(c)** flexural-tensile stiffness modulus SB.

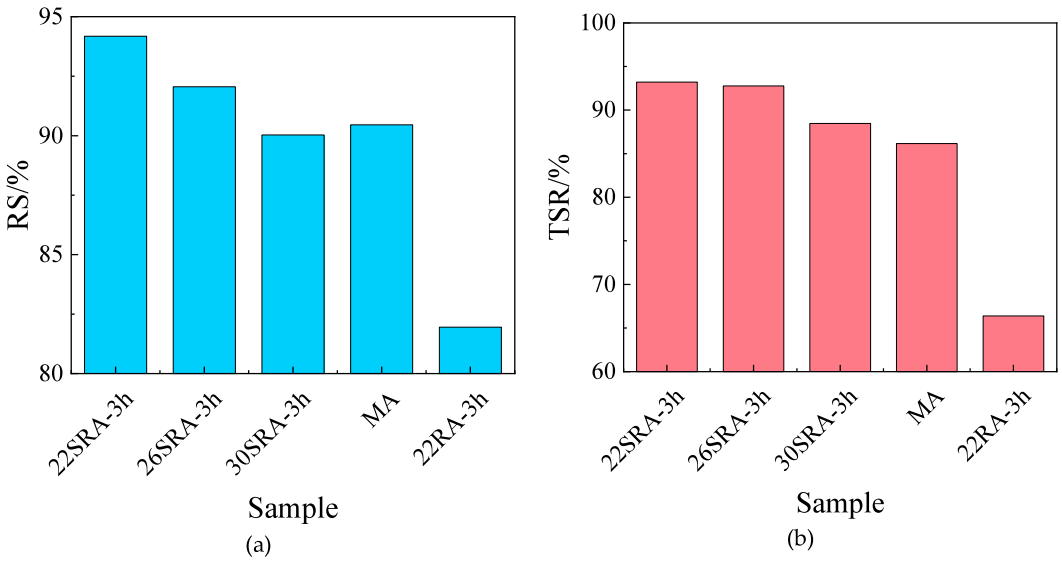

FIGURE 25
Moisture susceptibility evaluation: **(a)** residual stability (RS); **(b)** tensile strength ratio (TSR) for different asphalt mixtures.

TABLE 11 Unit price of raw materials.

Material	Aggregate	Mineral filler	Base asphalt	Rubber powder	Cracking agent
Price (¥/t)	65	125	4,000	1,100	11,000

14, 19, and 22 and Tables 8 and 9, provide critical insights into the aging-induced performance evolution.

The 26SRA-3h binder demonstrated superior resistance to long-term aging. Specifically, it exhibited the smallest increase in the relaxation modulus G(60s) and the smallest reduction in the relaxation rate m(60s) at low temperature among all binders after PAV aging (Figure 22), indicating a well-preserved stress relaxation capacity. This is directly correlated with its outstanding retention of flexural tensile strain in the mixture low-temperature bending test (Figure 24). Similarly, the fatigue life (N_f) of 26SRA-3h experienced a less severe reduction (approximately 40%) after PAV aging compared to MA and 22RA-3h (Figure 19).

This enhanced aging resistance is mechanistically attributed to the unique microstructure of the devulcanized rubber asphalt. The controlled breakdown of the rigid rubber network into a finely dispersed, elastic phase within the asphalt matrix creates

TABLE 12 Material consumption and cost comparison of different asphalt mixtures.

Mixture parameter	MA mixture	22RA-3h mixture	26SRA-3h mixture
Optimal binder content (%)	5.1	6.6	6.0
Asphalt content (%)	4.85	6.19	5.66
Mixture density (g/cm^3)	2.47	2.40	2.44
Mixture quantity (t)	1,108	1,080	1,095
Base asphalt (t)	53.7	51.2	47.3
Mineral filler (t)	63.2	61.0	61.8
Aggregate (t)	991.1	952	968.9
Rubber powder (t)	0	15.8	17.5
Cracking agent (t)	0	0	0.33
Cost (10,000 ¥)	28.4	29.1	27.6

a more homogeneous system. This structure mitigates the formation of a continuous brittle phase upon oxidation. The FTIR evidence (Section 3.1.1) supports this by showing the generation of flexible olefinic structures during devulcanization. Therefore, the macroscopic performance retention after long-term aging can be qualitatively correlated to this stabilized microarchitecture, which effectively retards the hardening and embrittlement processes common in conventional asphalts during oxidative aging.

4 Conclusion

This study establishes a comprehensive framework for the molecular-to-macroscopic engineering of high-performance, high-content rubberized asphalt. The core innovation lies in the precise modulation of the devulcanization process to dictate the material's microstructure, which in turn governs its macroscopic performance. The main findings are as follows:

1. This work designed and developed a novel devulcanizing agent (RubberSynth-AP) and a controlled process, achieving an unprecedented rubber content of 30% and identifying a performance optimum at the 26% formulation. This optimal formulation delivers a synergistic combination of properties: a failure temperature of 76.5 °C, a 40% reduction in viscosity, a recovery rate of 53.12%, and a non-recoverable creep compliance of 1.268 kPa^{-1}.
2. The underlying mechanisms were deciphered, demonstrating that controlled devulcanization transforms rigid rubber particles into a soft, reinforcing phase. This transformation enables a paradigm shift from gap-graded to superior continuous dense-graded mixtures (AC-13), achieving a dynamic stability of 3,850 cycles/mm.
3. A key trade-off was revealed and effectively addressed: the process simultaneously enhances fatigue life by 300% and low-temperature flexural strain by 50%, while the associated aging sensitivity was also quantified and mechanistically explained. The 26% formulation was identified as the optimal compromise.
4. The technology demonstrates compelling sustainability, enabling the consumption of 18 tons of waste rubber per lane-kilometer while reducing material costs by approximately ¥17,000, thereby transforming an environmental burden into a high-value engineering asset.

This work provides not merely a new material, but a foundational blueprint for de-signing next-generation pavement materials through targeted microstructural engineering. It thereby bridges the critical gap between advanced material science and sustainable infrastructure practice.

5 Limitations and future research

This study has some limitations that should be acknowledged. The research was conducted primarily on laboratory-scale specimens and focused on a single dense-graded mixture type (AC-13). The aging conditions, while representative, were limited to standard laboratory protocols. Based on these limitations, several important research directions are recommended for future work. First, the performance of the developed asphalt binder should be evaluated with different aggregate gradations, including both fine-graded and coarse-graded mixtures, to assess its versatility across various pavement designs. Second, comprehensive long-term performance studies are needed, including the effects of extended aging on both the binder and mixture performance under realistic environmental conditions. Field validation through test sections would be particularly valuable to confirm the laboratory findings. Although the long-term aging behavior was evaluated via PAV tests and mechanistically discussed through rheological and spectroscopic (FTIR) data, establishing a quantitative correlation between the evolution of asphalt chemical components (e.g., saturates, aromatics, resins, asphaltenes) and

macroscopic performance decay remains a valuable objective for future research. Other promising research directions include investigating the material's performance under extreme climate conditions and developing optimized production parameters for large-scale implementation.

Data availability statement

The original contributions presented in the study are included in the article/supplementary material, further inquiries can be directed to the corresponding author.

Author contributions

MY: Conceptualization, Writing – review and editing. SL: Conceptualization, Supervision, Writing – review and editing. XG: Methodology, Writing – review and editing. MP: Writing – review and editing. CL: Writing – review and editing. OX: Investigation, Writing – review and editing. SW: Validation, Writing – review and editing. CJ: Funding acquisition, Methodology, Supervision, Writing – review and editing. YL: Formal Analysis, Writing – original draft, Writing – review and editing. HM: Formal Analysis, Writing – review and editing. LZ: Validation, Writing – review and editing. WA: Investigation, Writing – review and editing.

Funding

The authors declare that financial support was received for the research and/or publication of this article. This research was funded by the Department of Transport of Qinghai Province, China, grant number 2025-01; the Department of Science and Technology of Inner Mongolia Autonomous Region, China, grant number 2025YFKL0016; the Department of Science and Technology of Gansu Province, China, grant number 25YFFA078; and the Department of Transport of Gansu Province, China, grant number 2025-HEFJ-QT07.

Conflict of interest

The authors declare that the research was conducted in the absence of any commercial or financial relationships that could be construed as a potential conflict of interest.

Generative AI statement

The authors declare that no Generative AI was used in the creation of this manuscript.

Any alternative text (alt text) provided alongside figures in this article has been generated by Frontiers with the support of artificial intelligence and reasonable efforts have been made to ensure accuracy, including review by the authors wherever possible. If you identify any issues, please contact us.

Publisher's note

References

Arabani, M., Tahami, S. A., and Hamedi, G. H. (2018). Performance evaluation of dry process crumb rubber-modified asphalt mixtures with nanomaterial. *Road. Mater. Pavement Des.* 19 (5), 1241–1258. doi:10.1080/14680629.2017.1302356

Duan, K., Wang, C., Liu, J., Song, L., Chen, Q., and Chen, Y. (2022). Research progress and performance evaluation of crumb-rubber-modified asphalts and their mixtures. *Constr. Build. Mater.* 361, 129687. doi:10.1016/j.conbuildmat.2022.129687

Gamboa, C. J. O., Ruiz, P. A. C., Kaloush, K. E., and Linares, J. P. L. (2021). Life cycle assessment including traffic noise: conventional vs. rubberized asphalt. *Int. J. Life Cycle Assess.* 26 (12), 2375–2390. doi:10.1007/s11367-021-01992-0

Gao, L., Zhu, X., Zhang, P., Cai, N., Li, L., and He, R. (2025). Desulphurisation of waste rubber powder using mechanochemical method and the influence on modified asphalt. *Road. Mater. Pavement Des.* 26 (1), 1–18. doi:10.1080/14680629.2024.2335190

Gkyrtis, K., and Pomoni, M. (2024). An overview of the recyclability of alternative materials for building surface courses at pavement structures. *Buildings* 14 (6), 1571. doi:10.3390/buildings14061571

Han, L., Zheng, M., and Wang, C. (2016). Current status and development of terminal blend tyre rubber modified asphalt. *Constr. Build. Mater.* 128, 399–409. doi:10.1016/j.conbuildmat.2016.10.080

Kabir, S. F., Zheng, R., Delgado, A. G., and Fini, E. H. (2021). Use of microbially desulfurized rubber to produce sustainable rubberized bitumen. *Resour. Conserv. Recycl.* 164, 105144. doi:10.1016/j.resconrec.2020.105144

Li, Y., Zhao, C., Li, R., Zhang, H., He, Y., Pei, J., et al. (2025). Dry-process reusing the waste tire rubber and plastic in asphalt: modification mechanism and mechanical properties. *Constr. Build. Mater.* 458, 139759. doi:10.1016/j.conbuildmat.2024.139759

Liu, Z., Zhou, Z., Gu, X., Sun, L., and Wang, C. (2023). Laboratory evaluation of the performance of reclaimed asphalt mixed with composite crumb rubber-modified asphalt: reconciling relatively high content of RAP and virgin asphalt. *Int. J. Pavement Eng.* 24 (1), 2217320. doi:10.1080/10298436.2023.2217320

Obukhova, S., Budkina, A., Korolev, E., and Gladkikh, V. (2024). Impacts of waste rubber products on the structure and properties of modified asphalt binder: part II—Rubber reclaim. *Materials* 17 (20), 5091. doi:10.3390/ma17205091

Payungwong, N., Wu, J., and Sakdapipanich, J. (2024). Unlocking the potential of natural rubber: a review of rubber particle sizes and their impact on properties. *Polymer* 308, 127419. doi:10.1016/j.polymer.2024.127419

Picado-Santos, L. G., Capitão, S. D., and Neves, J. M. C. (2020). Crumb rubber asphalt mixtures: a literature review. *Constr. Build. Mater.* 247, 118577. doi:10.1016/j.conbuildmat.2020.118577

Putra Jaya, R., Abdul Hassan, N., and Erdem, S. (2021). Editorial: trends and advanced materials for pavement and road infrastructure. *Front. Mater.* 8, 762864. doi:10.3389/fmats.2021.762864

Qiao, K., Tang, N., Yuan, C., Li, R., Zhu, H., Wang, L., et al. (2025). Rheological properties and storage stability of high content rubber modified asphalt. *Constr. Build. Mater.* 489, 142129. doi:10.1016/j.conbuildmat.2025.142129

Sienkiewicz, M., Borzędowska-Labuda, K., and Wojtkiewicz, A. (2017). Development of methods improving storage stability of bitumen modified with ground tire rubber: a review. *Fuel Process. Technol.* 159, 272–279. doi:10.1016/j.fuproc.2017.01.049

Su, J., Li, P., Zhu, G., Wang, X., and Dong, S. (2024). Interface interaction of waste rubber–asphalt system. *Buildings* 14 (6), 1868. doi:10.3390/buildings14061868

Wang, S., Cheng, D., and Xiao, F. (2017). Recent developments in the application of chemical approaches to rubberized asphalt. *Constr. Build. Mater.* 131, 101–113. doi:10.1016/j.conbuildmat.2016.11.077

Wang, G., Wang, X., Lv, S., Qin, L., and Peng, X. (2020). Laboratory investigation of rubberized asphalt using high-content rubber powder. *Materials* 13 (19), 4437. doi:10.3390/ma13194437

Wang, S., Huang, W., Liu, X., and Lin, P. (2022). Influence of high content crumb rubber and different preparation methods on properties of asphalt under different aging conditions: chemical properties, rheological properties, and fatigue performance. *Constr. Build. Mater.* 327, 126937. doi:10.1016/j.conbuildmat.2022.126937

Wang, S., Kang, A., and Huang, W. (2024a). Evaluation of the properties of high-content degraded crumb rubber–modified asphalt under thermal oxidation and weathering aging. *Sci. Total Environ.* 955, 177104. doi:10.1016/j.scitotenv.2024.177104

Wang, C., Tian, X. G., Wang, Y., and Li, G.(2024b). Asphalt aging and its anti-aging mechanism based on quantum chemistry. *Case Stud. Constr. Mater.* 20, e02802. doi:10.1016/j.cscm.2023.e02802

Wu, Z., Ge, D., Ju, Z., and Xue, Y. (2023). The performance evaluation of extracted asphalt binder from dry process produced rubber modified asphalt mixture. *Constr. Build. Mater.* 401, 131864. doi:10.1016/j.conbuildmat.2023.131864

Xu, G., Yu, Y., Yang, J., Wang, T., Kong, P., and Chen, X. (2021). Rheological and aging properties of composite modified bitumen by styrene–butadiene–styrene and desulfurized crumb rubber. *Polymers* 13 (18), 3037. doi:10.3390/polym13183037

Xu, G., Yao, Y., Ma, T., Hao, S., and Ni, B. (2023). Experimental study and molecular simulation on regeneration feasibility of high-content waste tire crumb rubber modified asphalt. *Constr. Build. Mater.* 369, 130570. doi:10.1016/j.conbuildmat.2023.130570

Yang, Z., Wang, L., Bin, X., Cao, D., Li, J., and Zhao, K. (2022). Performance of SBS modifier-crumb rubber composite modified asphalt used as an anti-wear layer of perpetual pavement. *Int. J. Pavement Eng.* 23 (12), 4097–4111. doi:10.1080/10298436.2021.1932882

Yao, H., Dan, H. C., Liu, K., and Meng, W. (2023). Editorial: "functional pavement and advanced material testing technology". *Front. Mater.* 9, 1117075. doi:10.3389/fmats.2022.1117075

Zhang, B., Chen, H., Zhang, H., Kuang, D., Wu, J., and Zhang, X. (2019). A study on physical and rheological properties of rubberized bitumen modified by different methods. *Materials* 12 (21), 3538. doi:10.3390/ma12213538

Zhang, H., Zhang, Y., Chen, J., Liu, W., and Wang, W. (2022). Effect of desulfurization process variables on the properties of crumb rubber modified asphalt. *Polymers* 14 (7), 1365. doi:10.3390/polym14071365

Zhang, S., Yang, Y., Guo, R., Yan, Y., Huan, H., and Wan, B.(2023a). Study on the low-temperature pre-desulfurization of crumb rubber-modified asphalt. *Polymers* 15(10), 2273. doi:10.3390/polym15102273

Zhang, L., Wang, H., Zhang, C., and Wang, S. (2023b). Laboratory testing and field application of devulcanized Rubber/SBS composite modified asphalt. *Case Stud. Constr. Mater.* 19, e02285. doi:10.1016/j.cscm.2023.e02285

Zhang, Y., Ding, P., Zhang, L., Luo, X., Cheng, X., and Zhang, H. (2024a). Green roads ahead: a critical examination of bio-bitumen for sustainable infrastructure. *Front. Mater.* 11, 1382014. doi:10.3389/fmats.2024.1382014

Zhang, H., Zhang, Y., Chen, J., Liu, W., and Wang, W.(2024b). Influence of preparation parameters on rheological properties and relation analysis of waste rubber modified bitumen mastic. *Front. Mater.* 11, 1435814. doi:10.3389/fmats.2024.1435814

Zhang, H., Lv, S., Pang, J., Chen, J., and Xuan, W.(2024c). Effects of aging on rheological properties and microstructural evolution of SBS modified asphalt and crumb rubber modified asphalt binders. *Buildings* 14(6), 1722. doi:10.3390/buildings14061722

Zhao, Z., Wu, S., Xie, J., Yang, C., Yang, X., Wang, F., et al. (2023). Utilization of high contents desulfurized crumb rubber in developing an asphalt rubber pellets modified asphalt. *Constr. Build. Mater.* 402, 133043. doi:10.1016/j.conbuildmat.2023.133043

Zhao, W., Geng, J., Niu, Y., Wang, W., Li, X., Chen, M., et al. (2024). Mechanisms associated with sulfidation gas release, desulphurisation and degradation of rubber powder in crumb rubber modified asphalt. *Int. J. Pavement Eng.* 25 (1), 2339997. doi:10.1080/10298436.2024.2339997

Zhou, Y., Lu, Q., Cheng, Z., Wang, J., Zhong, J., Lu, Q., et al. (2024a). Synergy of devulcanized rubber and rock asphalt for asphalt modification. *Case Stud. Constr. Mater.* 21, e03432. doi:10.1016/j.cscm.2024.e03432

Zhou, Y., Xu, G., and Wang, H. (2024b). Investigation of the rheological properties of devulcanized rubber-modified asphalt with different rubber devulcanization degrees and rubber contents. *Road. Mater. Pavement Des.* 25 (9), 1950–1963. doi:10.1080/14680629.2023.2287714

Zhou, Y., Fan, Y., Xu, G., Gong, M., Chen, X., Yang, J., et al. (2025). Aging behavior of desulfurized rubber-modified asphalt: evolution of rheological properties and mechanistic interpretation. *J. Mater. Civ. Eng.* 37 (10), 04025355. doi:10.1061/JMCEE7.MTENG-20267